UAB
Universitat Autònoma de Barcelona

UAB

Universitat Autònoma de Barcelona

Department of Chemistry
Faculty of science

Fast responsive photochromic materials through nanoemulsion entrapment

Héctor Torres Pierna

PhD Thesis
PhD in Material Science
2019

Supervisor:

Dr. Claudio Roscini

Tutor:

Prof. Jordi Hernando Campos

ICN2

EXCELENCIA
SEVERO
OCHOA

Institut Català
de Nanociència
i Nanotecnologia

Memòria presentada per aspirar al Grau de Doctor per:

Héctor Torres Pierna

Vist i plau

Director:

Dr. Claudio Roscini

Tutor:

Prof. Jordi Hernando

Bellaterra, 03 de desembre, 2019.

To my family

"We are trying to prove ourselves wrong as quickly as possible, because only in that way can we find progress."

—Richard P. Feynman

"There is nothing like looking, if you want to find something. You certainly usually find something, if you look, but it is not always quite the something you were after."

—J.R.R. Tolkien, The Hobbit or There and Back Again

Preface:

This doctoral research has been performed under the scope of Industrial Doctorates Project. Financed by the Generalitat de Catalunya, the aim of this program is to promote technology transfer from public research centers and universities to private companies, to promote applied research and the launch of innovative products into de market.[1]

The research group where this work has been carried out is Nanostructured Functional Materials (Nanosfun), from the Catalan Institute of Nanoscience and Nanotechnology (ICN2), from which the thesis director Dr. Claudio Roscini is part.[2] The company involved in this project is Futurechromes S.L.., a start-up company created to exploit a technology previously developed in Nanosfun.[3]

This doctoral research was carried out by Héctor Torres Pierna, currently in possession of a MSc degree in Industrial Chemistry, and ascribed to the Materials Science PhD program, at the Universitat Autònoma de Barcelona,[4] under tuition of Prof. Jordi Hernando.
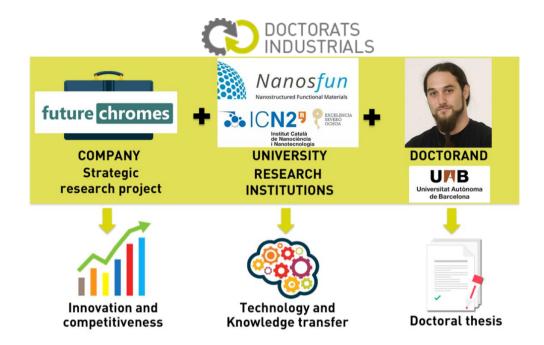
As direct outcome of this industrial doctorate project, by the time this dissertation is deposited, a patent has been filed and granted (US10227527B2), a scientific journal article is pending of publication, several prototypes produced, and important steps towards the commercialization of photochromic products based on the developed technology have been done.

---

[1] http://doctoratsindustrials.gencat.cat/en
[2] https://icn2.cat/en/nanostructured-functional-materials-group
[3] http://futurechromes.com/
[4] https://www.uab.cat/web/postgraduate/phds/all-phd-programmes/general-information/materials-science-1345467765430.html?param2=1345657420764

Industrial Doctorate Program Scheme

Acknowledgements:

First of all, I would like to acknowledge to the people that made this project possible. This starts by my PhD thesis director Dr. Claudio Roscini, who has invested brains, body and soul into this project, always having new insights and kind words to motivate me; and Prof. Daniel Ruiz-Molina, who with his knowledge and experience has paternally guided us in this project from its very beginning.

Also of crucial importance, I would like to thank to Aurora Conill and Piergiorgio Pelassa, for personally trusting in me and this project, and for their talent, competence and boldness in the industrial research, finances and business that they provided to this project. Thanks also to our industrial partners (confidential) for joining us and in this adventure.

Special acknowledgments also go to the lovely Dr. Nuria Vázquez-Mera and Prof. Jordi Hernando, for their original work on photochromic microcapsules that founded the grounds for this project 6 years ago, and for always having the perfect line to cheer up our moods.

I would like to also personally thank to Bea, Ayala, Pablo, Julià, Fernando, Josep, Noe, Jaume, 'Xiquet'... well, to ALL of my current and former partners in the Nanosfun research group, and also to Marcos Rosado, Javier Saiz and all the other ICN2 staff members who helped me along all these years. Thanks for your company and camaraderie, for all the coffees, for all the advices, for all whinings and laughters together.

Last, but not least at all, to my family. Thanks to my parents, for helping me in every step of my life journey and for their moral support; and of course, thanks to Dydy, for always supporting me with all her strengths, for believing in me every single day and for brightening my heart and my mind every day with her blue moonlight.

Contents

X

List of abbreviations:

Abs	Absorbance	**QUV**	Accelerated weathering tester
BA	Boric acid	**Rev.**	Vivimed Reversacol™
CQ	Camphorquinone	**Rev.Claret**	Claret
DSC	Differential scanning calorimetry	**Rev.Mid**	Midnight Grey
GA	Glutaraldehyde	**Rev.Misty**	Misty Grey
HD870	Hybridur® 870	**Rev.PP**	Palatinate Purple
HECell	Hydroxyethyl cellulose	**RI**	Refractive index
HPH	High pressure homogenization	**RIMA**	RI matching agent
M812	Migyol® 812	**SDS**	Sodium dodecyl sulfate
MC	Merocyanine	**SEM**	Scanning electron microscopy
ML7510	Mowilith® LDM 7510	**SP**	Spiro
Mw	Weight average molecular weight	**St.Dv.**	Standard deviation
NE	Nanoemulsion	**SW**	Smart Window
NEE	Nanoemulsion Entrapment	$t_{1/2}$	Fading half-lifetime
NIR	Near Infrared	$t_{3/4}$	Fading three-quarters-lifetime
O/W	Oil in water	**TAS**	Transient absorption spectroscopy
PAM	Polyacrylamide	T_d	Decomposition temperature
PhI	Photorome™ I	**TEOS**	Tetraethyl orthosilicate
PIA	Periodic acid	T_g	Glass transition temperature
PMMA	Poly(methyl methacrylate)	**TGA**	Thermogravimetric analysis
PSS	Photostationary state	T_m	Melting temperature
PVA	Poly(vinyl alcohol)	**W/O**	Water in oil
PVA 10-98	Mowiol® 10-98	**X@Y**	Dye X dissolved in matrix Y
PVA 40-88	Mowiol® 40-88	**X@Y@Z**	Dye X dissolved in oil Y, entrapped in matrix Z
PVA 4-88	Mowiol® 4-88	**XL**	Cross-linking
QCT	Accelerated condensation tester	**ΔOD**	Increment in optical density
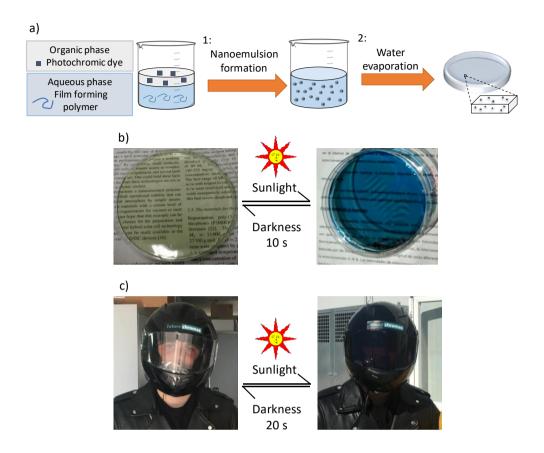
Abstract.

In this doctoral research, an optically transparent photochromic material with fast and liquid-like kinetic response has been developed, and the methodology to produce said material is described herein. This technology is based on the nanoemulsion entrapment (**NEE**) technique, in which an emulsion is first formed and stabilized by a film-forming polymer, and then the solvent of the continuous phase is removed, to generate a film containing the emulsion droplets entrapped in it.

Having the photochromic dyes dissolved in the dispersed liquid phase of the droplets ensures minimal steric hindrance for the dye to isomerize and therefore the fastest photochromic kinetics for the dye used (i.e. liquid-like behavior), while the continuous polymeric film provides a solid platform, which is the most convenient for the majority of applications. Moreover, the NEE films are visually transparent (> 90 %T), since the dispersed droplets are reduced to the nanoscale size (< 100 nm), by either ultrasonic irradiation or high pressure homogenization, minimizing light scattering.

Along this thesis it has been demonstrated that the properties of the NEE films are easily tunable to match the key requirements of different applications. By simply changing the photochromic dyes it is possible to control the photoinduced colors, the coloration/discoloration rates and the color intensity of the activated state. The coloration and discoloration rates can be finely tuned by substituting the hydrophobic oil of the droplets. The modification of the polymeric matrix allowed to withstand moisture and higher temperatures exposure.

The production of NEE films was scaled up to the 200 g. Some working prototypes for potential industrial applications were produced such as eyewear, smart windows, car windshields and helmet visors, and are presented at the end of this thesis.

a)

| Organic phase
■ Photochromic dye | 1:
Nanoemulsion
formation | 2:
Water
evaporation |

| Aqueous phase
Film forming
polymer |

b)

Sunlight

Darkness
10 s

c)

Sunlight

Darkness
20 s

Schematic representation of the NEE films preparation process (a) example of a NEE film example exhibiting fast photochromism (b) photochromic helmet prototype (c).

Chapter 1

Introduction

1 Introduction

1.1 Photochromism

The photochromic phenomenon can be simply described as a reversible color change of a substance when exposed to light.[1]

In a more precise and complete definition, photochromism refers to the process in which a compound A undergoes a reversible reaction when irradiated with certain wavelength of light and becomes a compound B, which is thermodynamically less stable and present a different absorption spectrum (**Figure 1-1**). The back reaction to the more stable form A can be achieved by either irradiation with a different wavelength (P-type photochromism) or through thermal relaxation (T-type photochromism).[2]
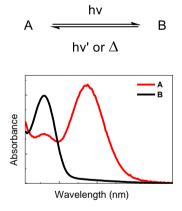
Figure 1-1: schematic representation of the photochromic process

Though this definition does usually refer to absorption changes in the visible range of the electromagnetic spectrum (λ = 400 - 750 nm), that produce color changes appreciable to the human eye, it does not exclude the cases when the spectral variation occur in the UV or the NIR range of the spectrum.[1]

Earliest reported examples of this photochromic substances date back to the 19th century, but the interest into this phenomenon increased exponentially since the

mid-20th century, when the glass manufacturing company Corning Inc. started to produce photochromic glasses based on silver halides,[3] the term "photochromism" was first proposed, and the synthetic methods to obtain organic photochromic compounds were improved.[1]

1.2 Applications of photochromic materials and products market

The reversible light-induced color change of photochromic materials is of great interest for the fabrication of light-responsive devices, such as optical filters, rewritable displays, optical memories, smart windows, smart biomaterials, etc.[4–11] Moreover, the two chemical species involved in the photochromic transition, not only differ in the color, but often also in physicochemical properties, such as geometry, polarity and functional groups, especially when using organic photochromic dyes.

This changes can be exploited to produce smart materials that change their wettability,[12] mechanical and thermal properties or pharmacological activity, actuators and molecular motors.[5,13] However, all of these applications are still under development in the academic community.

Regarding the industry, the photoinduced reversible coloration of T-type photochromic materials is what nowadays is mostly exploited. It is found in novelty items such as in toys and T-shirts, but it is in the eyewear industry where photochromic compounds are more broadly used.[14]

In fact, the global photochromic ophthalmic lenses market was valued around US$ 4.8 billion in 2018 and is projected to reach US$ 7.7 billion by 2024. This application represents the 80 % of all the photochromic dyes market.[15]

These products adapt to the different lighting conditions, turning dark when exposed to sunlight, and becoming clear when worn indoor, providing additional UV-protection and maximum comfort for the wearer. The main examples of photochromic lenses brands are Transitions™ by Transitions Optical,[16]

PhotoFusion® by Zeiss[17] and SunSensors™ by Mitsui (**Figure 1-2**).[18] Some other examples of commercial photochromic eyewear products are sunglasses, sport eyewear (e.g. Rockbros) and motorcycle helmet visors (e.g. from Lazer).
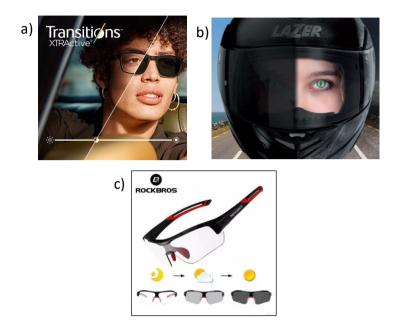
Figure 1-2: promotional images of photochromic commercial products: Transitions ophthalmic lenses (a),[16] Lazer helmet visor (b)[19] and Rockbros cycling sunglasses(c).[20]

A second potential application of photochromic compounds, which is attractive for the industry, is the field of smart windows (**SW**). This windows can adapt their clarity to the environmental conditions, increasing the comfort of the inhabitants, and potentially achieving energy savings, by reducing the heat gains and therefore air conditioning usage.[21,22]

The SW market was valued at 2.6 billion US$ in 2018 and is projected to reach 4.6 Billion US$ by 2025.[23] The SW market is currently dominated by electrochromic devices,[24] since they have superior performance.[21,25] Some main examples of electrochromic smart windows brands are SageGlass® by Saint-Gobain[26] and View®glass, acquired by Corning.[27]

However, photochromic SW could potentially achieve a share of the market, due to the simplicity and lower costs of the glass panels installation and maintenance, as it does not require wirelines nor power supply.[28] Nowadays, the photochromic SW are mainly under academic development,[11,25,29–31] though small companies already exists (e.g. CoolVu[32] and Tintdepot[33]) that sell add-on photochromic films for windows and windshields (**Figure 1-3**).
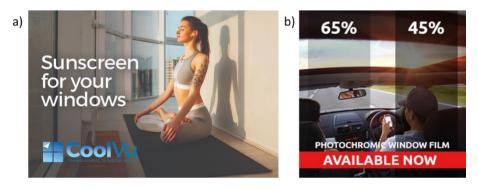
Figure 1-3: promotional images of photochromic add-on films for smart windows (CoolVU[32], a) and windshields (Tintdepot[33], b).

1.3 T-type photochromic dyes

Among the photochromic compounds, organic photochromic dyes are the most predominant for ophthalmic lenses.[34] These dyes have broad commercial availability, good fatigue resistance, photochromic response tunability (e. g. color type and intensity of the activated form, etc.) and good integrability into flexible, conformable plastic matrices (e.g. acrylates), which are the main material of the majority of lenses produced nowadays.[14,35]

Spirooxazines and naphthopyran derivatives are the most used T-type dyes in the industrial sector due to their enhanced fatigue resistance and scaled-up production.[6,34] These dyes reversibly interconvert from a thermodynamically stable colorless closed form (indoor) to a photoactivated merocyanine-like colored isomer when exposed to UV radiation (outdoors). The colored form reverts back to the

initial colorless state when the UV exposure is stopped, through spontaneous thermal relaxation (**Figure 1-4**).

The T-type photochromism of this family of dyes is suitable for light and cost-effective adaptive eyewear, since the materials made of these self-adapt to the lighting conditions without needing additional sensors nor power supply as electrochromic materials do.[36,37]

Figure 1-4: scheme of the photochromic interconversion of spirooxazines (a) and naphthopyrans (b).

1.4   Fast fading and matrix effect

Despite these dyes are already used in the ophthalmic industry, there are still important technical limitations that are preventing T-type photochromic materials to be used in more sectors. One of these is the fine control of the isomerization kinetics of the dyes, which is in general not easily achievable in solid matrices, where often significantly reduced light-induced coloration and thermal fading rates of the dyes are observed. This is due to the matrix effect.

The matrix effect is related to the steric hindrance that the solid matrix opposes to the conformation changes of the photochromic molecules involved during the photoinduced and thermal back isomerizations.[38] The more rigid and dense is a

polymer matrix, the higher is the steric hindrance and therefore, the slower is the interconversion rate. [39–41]

To solve this technical problem, during the latest years, researchers have been constantly coming up with new solutions, which could be classified in two different approaches.

One general strategy consists of the design and synthesis of new photochromic molecules that involve minimal conformational changes during the photochromic interconversions (e.g. molecules based on bridged imidazole dimers),[42–50] or prevent the formation of the longer-lived isomers of the open forms of spirooxazines (i.e. *trans*-merocyanines)[51,52] or naphthopyrans (i.e. *transoid-trans, TT*)[53–60] that slow down the ring-closure reaction (oxazines, substituted naphthopyrans) (**Figure 1-5**).
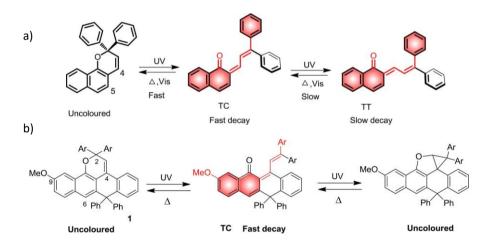
Figure 1-5: photochromic equilibrium between the closed form of naphtho[1,2-b]pyran and the two isomeric open forms TC (isomer that reverts faster to the colored form) and TT (slower isomer) (a); and the fused-naphthopyran that does not yield the slow component in the open form (b).[53]

Though this approach yielded photochromic dyes with very fast fading rates (from nanoseconds to seconds), it requires synthetic procedures, that difficult the tunability of the performances of the photochromic dyes and in some cases their commercialization. Moreover, while in some cases the open form concentration at

the photostationary state is too little to observe color formation, others still show a matrix effect and require plasticizers in the final films to preserve the solution behavior.

A second general strategy to minimize the matrix effect is to provide a soft or void environment to the photochromic dyes that oppose less steric hindrance and give free-volume for the photochromic molecule to isomerize and rotate. This has been achieved by different strategies, such as:

a) Functionalizing the photochromic molecules with flexible tails, that surround the photochromic moiety.[61–65]

b) Embedding the dyes in low glass transition (T_g) materials, such as polymers,[66] hybrid organic/inorganic materials,[67,68] or gels. [69–71]

c) Encapsulating the molecules in the cages of hybrid mesostructured (nano)materials,[72–76] metal-organic frameworks,[77,78] supramolecular cages[79–81] or liquid-core capsules[82,83]

Figure 1-6: strategies that minimize the matrix effect: molecular functionalization with flexible polymeric tails (a),[63] embedment of the dye in low T_g polymeric matrices (b)[66] and encapsulation of the dye into liquid-core microcapsules(c).[82]

Though these strategies improved the kinetic response of the photochromic dyes they still need chemical modification of the dyes or yield non-optically transparent films (key properties for optical filters applications).

1.5   Transparency and light scattering

The lack of optical transparency of the materials obtained with some of the above strategies is caused by the introduction of microscopic particles or domains of different materials (e.g. microcapsules) into the polymeric matrices, which generate light scattering at each interfaces

The amount of light scattered by these particles is proportional to their size, concentration, refractive index mismatch with the continuous matrix, and the specific wavelength of the incident light.[84]

As described by the Mie light scattering theory,[85] particles with size above 200 nm in diameter generally backscatter most of the visible light (λ = 400 - 700 nm), yielding opaque or very turbid dispersions. Dispersions with particles of size between 200 nm and 100 nm in diameter start to become partially transparent, allowing the transmission of longer wavelengths radiation (e.g. red light), but still significantly scattering shorter wavelengths (e.g. blue light) and therefore displaying a characteristic opalescence due to the Tyndall effect.[86] Suspensions of nanoparticles below 100 nm in diameter have high transmittance in the whole visible range, despite the refractive index mismatch or the concentration.

Therefore, when applying structured materials (e.g. the encapsulation strategy) to minimize the matrix effect, it is necessary to reduce the particles size to the nanoscale, in order to obtain a universally transparent photochromic material, suitable for optical applications such as eyewear and smart windows. This also applies to the strategy based on core-shell microcapsules that was recently developed in the Nanosfun group (**Figure 1-7**).[82] The films prepared through this

approach showed solution like and fast responsive photochromic properties, though they were highly opaque due the microcapsules size.
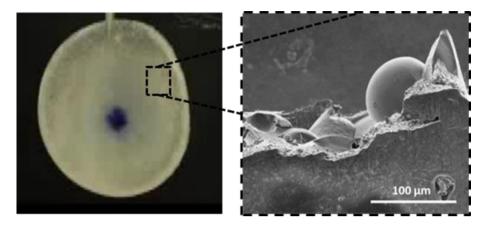
Figure 1-7: opaque film containing fast fading photochromic microcapsules.[82]

Though the preparation of such nanocomposites is possible,[87–91] they require time/cost-consuming syntheses, and are effective only under certain balance of hydrophilic/hydrophobic materials. Therefore, a universal and quick strategy to obtain transparent photochromic materials with fast and easily tunable photochromic response is still a challenge for their use in practical applications.

1.6   Nanoemulsion entrapment

To overcome these drawbacks, in this doctoral research a straightforward and universal solution is proposed. This strategy was inspired from technologies based on droplets trapped within a continuous polymer matrix (e.g. electronic papers,[92] photoprotective packaging,[93] liquid crystal displays and smart windows,[94] scratch-and-sniff coatings[95]).
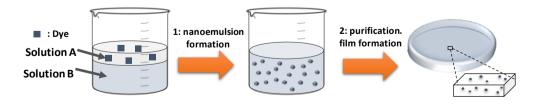
Figure 1-8: schematic representation of NEE films preparation procedure.

11

Again, these examples yield non-transparent films due to the light scattering caused by the micrometric droplet size contained. In order to achieve visual transparency of these materials, the droplets of the emulsion must be reduced to the nanoscale.

Therefore, the preparation approach to achieve such films consisted in:

i.   the preparation of an oil-in-water (o/w) nanoemulsion made of hydrophobic nanodroplets (< 100 nm), containing the photochromic dye, dispersed in the water phase in the presence of a hydrophilic polymer that acts as both droplet stabilizer and film-forming material;

ii. forming a film through water evaporation, during which the nanodroplets remain stabilized from the coalescence (guaranteeing transparency) and physically trapped in a separated phase (assuring fast photochromism).

The advantages of use of this strategy over the encapsulation approach are, among others:

- The nanoemulsion and the film are obtained in a one-pot process.

- It involves minimal work up and purification.

- No chemical reactions that could irreversibly alter the photochromic dyes are required.

- No additional surfactants are required for the nanoemulsion since the film-forming polymer is acting as droplets stabilizer.

1.7   Nanoemulsions

Emulsions are dispersions of droplets of one liquid into another immiscible continuous liquid phase. They are usually composed of a hydrophobic oil dispersed in an aqueous solution (**O/W**) or an aqueous solution dispersed into a continuous oil phase (**W/O**).[96]

Typical emulsions have droplet sizes of about 0.5 µm in diameter or above and are visually opaque. These dispersions require energy input to be produced (e.g. shear forces) and are not thermodynamically stable, due to the increment of surface tension associated to the increasing oil-water interfacial area. The droplets have the tendency to flocculate or sediment and coalesce overtime, even if surfactants are added to reduce the surface tension (Kinetic instability).[97]

A particular type of emulsion is the nanoemulsion (**NE**), achieved when enough energy and surfactant are added, and the droplet sizes are reduced to the nanoscale (approximately 100 nm or below). Though these NE are still thermodynamically unstable, and often require high-energy input to be obtained, the flocculation and coalescence processes are very slow and therefore become kinetically stable even for several months. Moreover, NE are optically clearer due to the small size of the nanodroplets, which greatly reduces light scattering (**Figure 1-9**).[98] NE should not be confused with microemulsions, which are thermodynamically stable and do not require high energy input, but require a high concentration of surfactant to be achieved.[97]

Figure 1-9: transparent nanoemulsion (radius = 22 nm) and opaque microscale emulsion (radius 3.5 µm), at the same oil concentration in the water phase.[98]

NE can be prepared by a variety of methods, classified as low-energy or high-energy methods. Low-energy methods cleverly exploit the potential energy of

specific chemical compositions, that is released as a phase change is performed. A major example of this is the phase inversion composition method, in which normally a W/O emulsion is converted into an O/W nanoemulsion by constantly adding water dropwise (**Figure 1-10**). However, these methods are too dependent on the mixture formulation, and difficult to scale up in a controlled manner.[99]
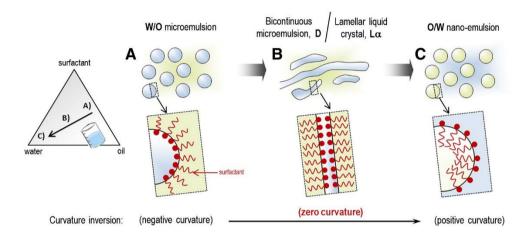
Figure 1-10: schematic representation of the phase inversion composition nanoemulsification process.[99]

On the contrary, high-energy methods rely on instruments with great power output, such as ultrasonicators, high-pressure homogenizators and microfluidic devices, that breaks large droplet into nanodroplets. The ultrasonic irradiation produces acoustic cavitation fields,[100] while the high pressure homogenizations and microfluidic devices force the emulsions to pass through microsized channels, producing impact of droplets against the channel walls, high-shear forces and extreme elongation of the droplets (**Figure 1-11**).[101,102]
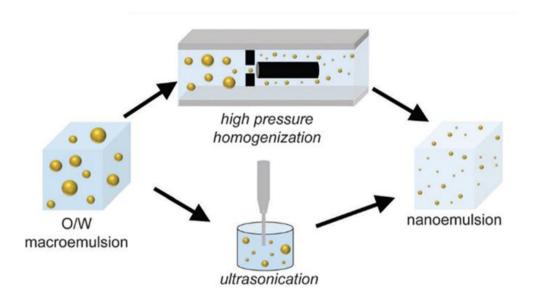
Figure 1-11: schematic representation of high-energy nanoemulsification methods.[101]

For this doctoral research, nanoemulsions prepared by high-energy methods were selected over low-energy produced nanoemulsions and microemulsions due to the more robust formulation and easiest scalability for the industry.[103,104]

1.8 References:

[1] H. Bouas-Laurent, H. Dürr, *Pure Appl. Chem.* **2001**, *73*, 639.

[2] P. Bamfield, M. G. Hutchings, *Chromic Phenomena*, Royal Society Of Chemistry, Cambridge, **2010**.

[3] W. H. Armistead, S. D. Stookey, **Science**, **1964**, *144*, 150.

[4] J. Boelke, S. Hecht, *Adv. Opt. Mater*. **2019**, *7*, 1900404.

[5] H. Nie, J. L. Self, A. S. Kuenstler, R. C. Hayward, J. Read de Alaniz, *Adv. Opt. Mater.* **2019**, *7*, 1900224.

[6] V. A. Barachevsky, *J. Photochem. Photobiol. A Chem.* **2018**, *354*, 61.

[7] J. Zhang, J. Wang, H. Tian, *Mater. Horizons* **2013**, *1*, 169.

[8] J. Zhang, Q. Zou, H. Tian, *Adv. Mater.* **2013**, *25*, 378.

[9] G. Berkovic, V. Krongauz, V. Weiss, *Chem. Rev.* **2000**, *100*, 1741.

[10] M. Irie, *Chem. Rev.* **2000**, *100*, 1683.

[11] M. Hočevar, U. Opara Krašovec, *Sol. Energy Mater. Sol. Cells* **2018**, *186*, 111.

[12] L. Shuiping, T. Lianjiang, H. Weili, L. Xiaoqiang, C. Yanmo, *Mater. Lett.* **2010**, *64*, 2427.

[13] M. Irie, T. Fukaminato, K. Matsuda, S. Kobatake, *Chem. Rev.* **2014**, *114*, 12174.

[14] S. Nigel Corns, S. M. Partington, A. D. Towns, *Color. Technol.* **2009**, *125*, 249.

[15] TechSci Research, "Global Photochromic Lens Market By Material (Plastic, Polycarbonate & Glass), By Technology (In-Mass & Imbibing & Trans Bonding), By Application (Corrective & Preventive), By Distribution Channel, By Region, Competition, Forecast & Opportunities, 2024," can be found under https://www.techsciresearch.com/report/photochromic-lens-market/3486.html, last access: November **2019**.

[16] "Lentes Transitions XTRActive, Lentes fotocrómicas extraoscuras," can be found under https://www.transitions.com/es/productos/lentes-transitions-xtractive/, last access: November **2019**.

[17] Zeiss, "ZEISS PhotoFusion," can be found under https://www.zeiss.es/vision-care/para-profesionales-de-la-vision/productos/lentes-solares-y-filtros/lentes-fotosensibles/photofusion-old.html, last access: November **2019**.

[18] I. Mitsui Chemicals, "SunSensorsTM - An in-mass photochromic technology and brand," can be found under https://www.mitsuichemicals.com/sunsensors.htm, last access: November **2019**.

[19] "A History of Innovations, Lazer Helmets - Protect your freedom," can be found under https://www.lazerhelmets.com/brand.php, last access: November **2019**.

[20] "RockBros Unisex Photochromic Cycling Sunglasses UV Protection for Outdoor Sport Black Blue : Sports & Outdoors," can be found under https://www.amazon.com/RockBros-Photochromic-Sunglasses-Protection-Outdoor/dp/B0719FN4LM, last access: November **2019**.

[21] M. Mahdavinejad, M. Bemanian, N. Khaksar, *Int. Conf. Comput. Commun. Manag.* **2011**, *5*, 335.

[22] A. Piccolo, F. Simone, *J. Build. Eng.* **2015**, *3*, 94.

[23] Research Reports world, "Global Smart Windows Market Insights Forecast To 2025 – Research Reports World," can be found under https://www.researchreportsworld.com/global-smart-windows-market-insights-forecast-to-2025-14774707, last access: November **2019**.

[24] n-tech, "Smart Windows Materials Market Analysis: 2017 - 2026," can be found under https://www.ntechresearch.com/market-reports/smart-windows-materials/, last access: November **2019**.

[25] Y. Wang, E. L. Runnerstrom, D. J. Milliron, *Annu. Rev. Chem. Biomol. Eng.* **2016**, *7*, 283.

[26] Saint-Gobain, "Global Electrochromic Glass Provider, Dynamic Glass | SageGlass," can be found under https://www.sageglass.com/eu, last access: November **2019**

[27] View, "Electrochromic (Smart Glass) Technology, Product - View, Inc.," can be found under https://view.com/product/, last access: November **2019**.

[28] n-tech research, "Do Photochromic Materials Have a Chance in Windows Market?," can be found under https://www.ntechresearch.com/blog/photochromic-windows-market/, last access: November **2019**

[29] M. Hočevar, S. Bogati, A. Georg, U. O. Krašovec, *Sol. Energy Mater. Sol. Cells* **2017**, *171*, 85.

[30] L. Y. L. Wu, Q. Zhao, H. Huang, R. J. Lim, *Surf. Coatings Technol.* **2017**, *320*, 601.

[31] R. Tällberg, B.P. Jelle, R. Loonen, T. Gao, M. Hamdy, *Sol. Energy Mater. Sol. Cells* **2019**, *200*, 109828.

[32] Coolvu, "Transitional Window Film – CoolVu," can be found under https://www.coolvuwindowfilm.com/photochromic-transitional-window-film/, last access: November **2019**.

[33] Tintdepot.com, "Photochromic Window Film (Transitional)," can be found under https://tintdepot.com/product/photochromic-window-film-2/, last access: November **2019**

[34] J. C. Crano, R. J. Guglielmetti, in *Org. Photochromic Thermochromic Compd.* (Eds.: J.C. Crano, R. J. Guglielmetti), Plenum Press, New York, **1999**.

[35] S. Meir, in *Photochromic Mater. Prep. Prop. Appl.* (Ed.: Tian, H. and Zhang, J.), WILEY-VCH Verlag, **2016**, pp. 393–415.

[36] C. M. Lampert, *Mater. Today* **2004**, *7*, 28.

[37] P. Chandrasekhar, B. J. Zay, E. J. Laganis, V. V. Romanov, A. J. LaRosa, *Electrochromic Eyewear*, **2016**, US9482880B1.

[38] V. Pimienta, D. Lavabre, G. Levy, A. Samat, R. Guglielmetti, J. C. Micheau, *J. Phys. Chem.* **1996**, *100*, 4485.

[39] R. Pardo, M. Zayat, D. Levy, *Chem. Soc. Rev.* **2011**, *40*, 672.

[40] H. Torres-Pierna, C. Roscini, A. Vlasceanu, S. L. Broman, M. Jevric, M. Cacciarini, M. B. Nielsen, *Dyes Pigm.* **2017**, *145*, 359.

[41] G. Favaro, F. Ortica, A. Romani, P. Smimmo, *J. Photochem. Photobiol., A.* **2008**, *196*, 190.

[42] Y. Kishimoto, J. Abe, *J. Am. Chem. Soc.* **2009**, *131*, 4227.

[43] K. Mutoh, M. Sliwa, E. Fron, J. Hofkens, J. Abe, *J. Mater. Chem. C* **2018**, *6*, 9523.

[44] Y. Kobayashi, K. Mutoh, J. Abe, *J. Phys. Chem. Lett.* **2016**, *7*, 3666.

[45] A. Kimoto, A. Tokita, T. Horino, T. Oshima, J. Abe, *Macromolecules* **2010**, *43*, 3764.

[46] K. Yamamoto, K. Mutoh, J. Abe, *J. Phys. Chem. A* **2019**, *123*, 1945.

[47] R. Li, H. Ara, Y. Kobayashi, K. Mutoh, J. Abe*, Mater. Chem. Front.* **2019**, *3*, 2380.

[48] S. Toshimitsu, K. Shima, K. Mutoh, Y. Kobayashi, J. Abe, *ChemPhotoChem* **2019**, *3*, 487.

[49] A. Tokunaga, K. Mutoh, T. Hasegawa, J. Abe, *J. Phys. Chem. Lett.* **2018**, *9*, 1833.

[50] Y. Kobayashi, Y. Mishima, K. Mutoh, J. Abe, *Chem. Commun.* **2017**, *53*, 4315.

[51] M. Tomasulo, S. Sortino, F. M. Raymo, *Adv. Mater.* **2008**, *20*, 832.

[52] M. Tomasulo, S. Sortino, A. J. P. White, F. M. Raymo, *J. Org. Chem.* **2005**, *70*, 8180.

[53] C. M. Sousa, J. Berthet, S. Delbaere, P. J. Coelho, *Dyes. Pigm.* **2019**, *169*, 118.

[54] C. M. Sousa, J. Berthet, S. Delbaere, A. Polónia, P. J. Coelho, *J. Org. Chem.* **2015**, *80*, 12177.

[55] C. M. Sousa, J. Berthet, S. Delbaere, P. J. Coelho, *J. Org. Chem.* **2012**, *77*, 3959.

[56] C. M. Sousa, J. Pina, J. S. De Melo, J. Berthet, S. Delbaere, P. J. Coelho, *Org. Lett.* **2011**, *13*, 4040.

[57] B. Li, Z. Sun, Y. Zhai, J. Jiang, Y. Huang, J. Meng, *Tetrahedron* **2019**, *75*, 130471.

[58] H. Kuroiwa, Y. Inagaki, K. Mutoh, J. Abe, *Adv. Mater.* **2019**, *31*, 1.

[59] Y. Inagaki, Y. Kobayashi, K. Mutoh, J. Abe, *J. Am. Chem. Soc.* **2017**, *139*, 13429.

[60] C. M. Sousa, J. Berthet, S. Delbaere, A. Polónia, P. J. Coelho, *J. Org. Chem.* **2017**, *82*, 12028.

[61] T. Gushiken, M. Saito, T. Ubukata, Y. Yokoyama, *Photochem. Photobiol. Sci.* **2010**, *9*, 162.

[62] N. Malic, I. J. Dagley, R. A. Evans, *Dyes. Pigm.* **2013**, *97*, 162.

[63] F. Ercole, N. Malic, T. P. Davis, R. A. Evans, *J. Mater. Chem.* **2009,** *19*, 5612.

[64] R. A. Evans, T. L. Hanley, M. A. Skidmore, T. P. Davis, G. K. Such, L. H. Yee, G. E. Ball, D. A. Lewis, *Nat. Mater.* **2005**, *4*, 249.

[65] N. Malic, J. A. Campbell, A. S. Ali, C. L. Francis, R. A. Evans*, J. Polym. Sci., A.* **2011**, *49*, 476.

[66] W. Sriprom, M. Néel, C. D. Gabbutt, B. M. Heron, S. Perrier, J. Mater. Chem. **2007**, *17*, 1885.

[67] B. Schaudel, C. Guermeur, C. Sanchez, K. Nakatani, J. A. Delaire, J. Mater. Chem. **1997**, *7*, 61.

[68] J. Allouche, A. Le Beulze, J.-C. Dupin, J.-B. Ledeuil, S. Blanc, D. Gonbeau, *J. Mater. Chem.* **2010**, *20*, 9370.

[69] E. P. Y. Chow, J. Y. Ying, Y. S. Pek, *Fast-Response Photochromic Nanostructured Contact Lenses*, **2012**, US20120309761.

[70] Y. Yang, L. Guan, G. Gao, *ACS Appl. Mater. Interfaces* **2018**, *10*, 13975.

[71] D. Levy, *Chem. Mater.* **1997**, *9*, 2666.

[72] F. Ribot, A. Lafuma, C. Eychenne-Baron, C. Sanchez, *Adv. Mater.* **2002**, *14*, 1496.

[73] L. A. Mühlstein, J. Sauer, T. Bein, *Adv. Funct. Mater.* **2009**, *19*, 2027.

[74] L. Raboin, M. Matheron, J. Biteau, T. Gacoin, J.-P. Boilot, *J. Mater. Chem.* **2008**, *18*, 3242.

[75] N. Andersson, P. Alberius, J. Örtegren, M. Lindgren, L. Bergström, *J. Mater. Chem.* **2005**, *15*, 3507.

[76] G. Wirnsberger, B. J. Scott, B. F. Chmelka, G. D. Stucky, *Adv. Mater.* **2000**, *12*, 1450.

[77] D. E. Williams, C. R. Martin, E. A. Dolgopolova, A. Swifton, D. C. Godfrey, O. A. Ejegbavwo, P. J. Pellechia, M. D. Smith, N. B. Shustova, *J. Am. Chem. Soc.* **2018**, *140*, 7611.

[78] H. A. Schwartz, S. Olthof, D. Schaniel, K. Meerholz, U. Ruschewitz, *Inorg. Chem*. **2017**, *56*, 13100.

[79] D. Samanta, D. Galaktionova, J. Gemen, L. J. W. Shimon, Y. Diskin-Posner, L. Avram, P. Král, R. Klajn, *Nat. Commun.* **2018**, *9*, 2.

[80] D. Samanta, J. Gemen, Z. Chu, Y. Diskin-Posner, L. J. W. Shimon, R. Klajn, *Proc. Natl. Acad. Sci.* **2018**, *115*, 9379.

[81] A. M. Sanchez, R. H. De Rossi, *J. Org. Chem.* **1996**, *61*, 3446.

[82] N. Vázquez-Mera, C. Roscini, J. Hernando, D. Ruiz-Molina, *Adv. Opt. Mater.* **2013**, *1*, 631.

[83] S. Long, S. Bi, Y. Liao, Z. Xue, X. Xie, *Macromol. Rapid Commun.* **2014**, *35*, 741.

[84] David W. Hahn, "Light Scattering Theory," can be found under http://plaza.ufl.edu/dwhahn/Rayleigh%20and%20Mie%20Light%20Scattering.pdf, last access: November **2009**.

[85] C. F. Bohren, D. R. Huffman, *Absorption and Scattering of Light by Small Particles*, WILEY-VCH Verlag, **2004**.

[86] J. W. Gentry, *J. Aerosol Sci.* **1997**, *28*, 1365.

[87] H. Torres-Pierna, C. Roscini, J. Hernando Campos, *Fast Responsive Photochromic Materials Based on Polymeric Nanoparticles*, Master Thesis, Universitat Autònoma de Barcelona, **2014**.

[88] T. Feczkó, M. Kovács, B. Voncina, *J. Photochem. Photobiol., A* **2012**, *247*, 1.

[89] J. V. Valh, S. Vajnhandl, L. Š. I, A. Lobnik, M. Turel, B. Von I, *J. Nanomater*. **2017**, Article ID 4864760.

[90] Y. Wu, X. Qu, L. Huang, D. Qiu, C. Zhang, Z. Liu, Z. Yang, L. Feng, *J. Colloid Interface Sci.* **2010**, *343*, 155.

[91] L. L. Beecroft, C. K. Ober, *Chem. Mater.* **1997**, *9*, 1302.

[92] R. J. Paolini, D. D. Miller, B. Comiskey, J. M. Jacobson, B. Wu, C. Howie Honeyman, J. Lin, *Electrophoretic Medium and Process for the Production Thereof*, **2010**, US7848007B2.

[93] A. Morales, M. Á. Andrés, J. Labidi, P. Gullón, *Ind. Crops Prod.* **2019**, *131*, 281.

[94] P. S. Drzaic, *J. Appl. Phys.* **1986**, *60*, 2142.

[95] B. Duan, *Water and Heat-Resistant Scratch-and-Sniff Coatings*, **2013**, US8440265B2.

[96] IUPAC. Compendium of Chemical Terminology, 2nd ed. (the "Gold Book"). Compiled by A. D. McNaught and A. Wilkinson. Blackwell Scientific Publications, Oxford (**1997**). Online version (**2019-**) created by S. J. Chalk. ISBN 0-9678550-9-8. https://doi.org/10.1351/goldbook.

[97] J. Israelachvili, *Colloids Surf., A*, **1994**, *91*, 1.

[98] T. G. Mason, J. N. Wilking, K. Meleson, C. B. Chang, S. M. Graves, *J. Phys. Condens. Matter* **2006**, *18*, R635.

[99] C. Solans, I. Solé, *Curr. Opin. Colloid Interface Sci.* **2012**, *17*, 246.

[100] S. M. M. Modarres-Gheisari, R. Gavagsaz-Ghoachani, M. Malaki, P. Safarpour, M. Zandi, *Ultrason. Sonochem.* **2019**, *52*, 88.

[101] A. Gupta, H. B. Eral, T. A. Hatton, P. S. Doyle, *Soft Matter* **2016**, *12*, 2826.

[102] A. Gupta, H. B. Eral, T. A. Hatton, P. S. Doyle, *Soft Matter* **2016**, *12*, 1452.

[103] D. J. McClements, S. M. Jafari, in *Nanoemulsions Formul. Appl. Charact.*, Academic Press, **2018**, pp. 3–20.

[104] Y. Yang, C. Marshall-Breton, M. E. Leser, A. a. Sher, D. J. McClements*, Food Hydrocoll*. **2012**, *29*, 398.

Chapter 2

Objectives

2 Objectives

The main objective of this doctoral research is to develop a solid photochromic polymer material, with high transparency, solution-like and fast kinetic response.

The second objective of this thesis is to implement the so prepared photochromic materials into potential applications, such as smart windows and ophthalmic lenses, and achieve the commercialization of these innovative products.

The approach to achieve this material is based on the nanoemulsion entrapment (NEE) technology, which is a convenient, one-pot and reaction-free preparation process. Moreover, the preparation of such material has to be scalable, and requiring only easily available and commodity chemicals, suitable for the mass production.

To achieve these objectives, the following steps were taken:

- Demonstrate the viability of the NEE approach and show its potentiality in terms of photochromic performances tunability.
- Adapt the technology to the specific requirements of the different applications, such as high color intensity in the activated state, minimum residual color in the non-activated state, low haze, high moisture and fatigue resistance.
- Show the scalability of the nanoemulsion and NEE film preparation.
- Obtain working prototypes integrating the NEE photochromic films.

Chapter 3

NEE technology development

3   NEE technology development

3.1   Proof of concept

The viability of the nanoemulsion entrapment (**NEE**) technology to obtain transparent fast responsive photochromic films was proven by:

i. Preparing an oil-in water (O/W) nanoemulsion, where the oil phase was composed by a hydrophobic oil solution of the photochromic dye, while the water phase as an aqueous solution of a film forming polymer.

ii. Casting the solution onto a substrate and letting the water evaporate.

During the water evaporation it is expected the polymer precipitates forming the film and entrapping the nanodroplets in it. The main components selected for the proof of concept of the NEE film are presented below.

The selected photochromic dye was 1,3-dihydro-1,3,3-trimethylspiro[2H-indole-2,3'-[3H]naphth[2,1-b][1,4]oxazine], commercially known as Photorome I (**PhI**). This spirooxazine dye has a publically known chemical structure (**Figure 3-1**), is easily available from different distributors and has been previously used in Nanosfun research group as model photochromic dye.[1–4]

When a solution of this dye in a non-polar solvent (e.g. cyclohexane) is irradiated with UV light (λ_{max} = 360 nm), the colorless, thermodynamically stable spiro (**SP**) isomer interconverts to the merocyanine (**MC**). This form has an extended π-conjugated bonds, that originates a characteristic blue color (λ_{max} = 560 nm), (**Figure 3-2**). Once the irradiation is stopped, the MC form reverts gradually to the colorless SP by thermal relaxation. The fading kinetics of this process is strongly dependent on the surrounding medium properties, such as viscosity and polarity and gives information about the phase where the dye is dissolved in.[2,5–7]

Figure 3-1: molecular structure of the SP and photoinduced MC isomers of PhI. The MC isomer is reported as the contribution of the two resonance structures.
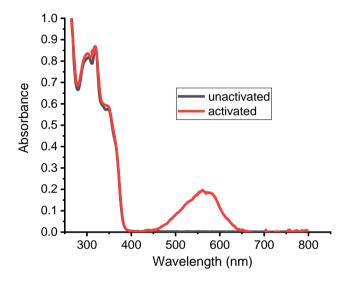
Figure 3-2: absorption spectra of the unactivated and photoactivated of PhI dissolved in cyclohexane at $5*10^{-4}$ M concentration.
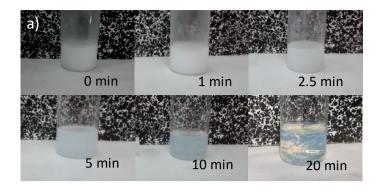
A coconut oil derivative branded as Miglyol® 812 (**M812**) was employed as oil carrier. This oil is widely used as hydrophic carrier of organic molecules (e.g. fragrances, drugs, etc.) for micro- and nanoencapsulation processes, since it is non-volatile, inexpensive and has low toxicity and high stability against oxidation. Moreover it is liquid at 0 °C,[2,8–10] ensuring a liquid environment for the dye, and thus liquid-like fading kinetics even in cold weathers. Its composition is a mixture of triglycerides from caprylic (approximately 50-65 %) and capric (approximately 30-45%) fatty acids.[11] PhI has an activated visual absorption at λ_{max} = 603 nm in M812.
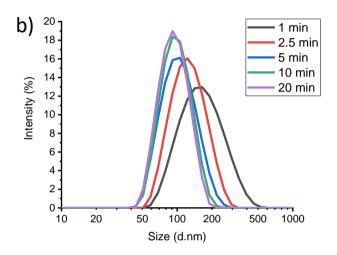
As for the matrix forming polymer, a low molecular weight and partially hydrolyzed polyvinyl alcohol (**PVA**), branded by the providers as the grade **4-88,** was chosen due to its high solubility in water and emulsification power.[12]

For the preparation of the NEE film, the PhI dye was dissolved into M812 oil at 1 wt.% concentration by magnetic stirring, while a 20 wt.% solution of PVA 4-88 was prepared by dissolving the polymer zin distilled water, under reflux. The organic photochromic solution and the polymeric aqueous phase were mixed in a 1:9 wt. ratio and magnetically stirred to achieve a white and opaque O/W preemulsion. This preemulsion was then subjected to ultrasonic irradiation to reduce the droplet size, whose evolution along time was monitored by Dynamic Light Scattering (**DLS**) at regular intervals of time until a plateau in droplet diameter was observed at 90 nm after 20 minutes of irradiation. The opacity of the nanoemulsion gradually decreased with the droplet size, reaching high visual transparency and a distinctive bluish coloration once the average droplet diameter decreased below 100 nm, due to the Tyndall effect (**Figure 3-3**).[13]

The resulting nanoemulsion was then coated on a polystyrene Petri plate substrate and the water was allowed to evaporate at 30 ºC under air atmosphere for 48 hours (**Figure 3-4**). As the water evaporates, the PVA precipitates trapping the lipophilic nanodroplets in it, generating the NEE film. The formulation of this nanoemulsion and the NEE film obtained from it were denoted as **PhI@M812@4-88**.

The transparency of the film is such that the letters of a text layered beyond the film can be clearly read. The fact that the film remains transparent indicated that the nanodroplets are not aggregating nor coalescing into larger droplets along the drying process.
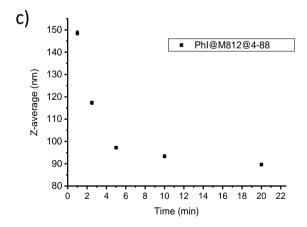
Figure 3-3: photographs of the nanoemulsion (a), DLS measurements of the nanoemulsion (b) and representation of the Z-average decrease (c) over time of sonication (0-20 min).

As a preliminary test, the presence of the photochromic dye in the film was confirmed by the development of the characteristic blue coloration of the photoactivated form of PhI upon irradiation of the NEE film with a UV mercury lamp (λ_{max} = 365nm) for 30 seconds. The fading of the blue color in the NEE film was fast and completed in less than 10 seconds, suggesting that PhI remained dissolved in the lipophilic nanodroplets along the ultrasonic irradiation and after the drying process of the film (**Figure 3-4**).

Liquid nanoemulsion		Solid NEE film		Photoactivated NEE film

Water evaporation

UV

10 s
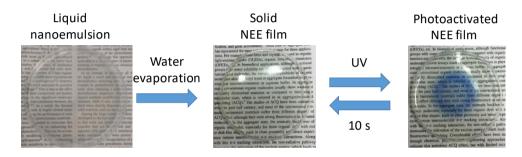
Figure 3-4: digital photographs of the casted liquid nanoemulsion, the dried NEE film and the photoinduced blue coloration of the NEE film.

3.2   NEE film characterization

3.2.1   Photochromic performance
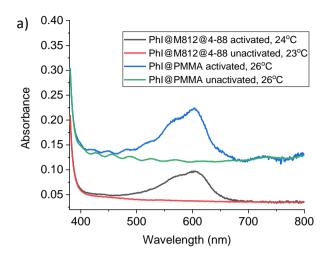
To assess the viability of NEE films as a fast photochromic material for optical applications, the photochromic performance of the above prepared film (**PhI@M812@4-88**) was determined by UV-vis transient absorption spectroscopy (**TAS**) and compared to a conventional photochromic film consisting of a solid solution of PhI in poly(methyl methacrylate) (**PhI@PMMA**). For the preparation of the PhI@PMMA film, see the experimental section (**Chapter 7.2**).

The experimental set-up consisted of placing the films in a custom holder for an Agilent Cary™ 60 UV-vis spectrophotometer. This spectrophotometer was chosen among other available equipment due to its robustness, simplicity of operation and its excellent scanning speed and time resolution (0.1s), which allows monitoring very

fast photochromic kinetic processes. Moreover, with this spectrophotometer it is possible to work with the open sample compartment, which permits the easy introduction of external UV-light sources, such a solar simulator, required for the characterization of photochromic samples, to better simulate their real performances when exposed to outdoors sunlight.

The sample holder of the spectrophotometer was also adapted in such a way that the film could be placed at a 90º angle respect to the measuring beam and at 45º respect to the excitation beam derived from the sun simulator. This specific set-up guarantees that the film can be simultaneously hit by the excitation beam (that activates the photochromism) and the measuring light (that measures the absorbance and transmission of the film) in the same spot. This configuration allows monitoring the time-dependent variation in light absorption/transmittance of the photochromic film before, during, and after (fading) the photoinduced isomerization.

The visible absorption spectra of the unactivated (residual absorption in the visible region and the colored (λ_{max} = 603 nm) forms of the films were measured in the dark and during irradiation, after reaching the photostationary state (**PSS**), respectively (**Figure 3-5, a**). To study the kinetic rate of the fading processes, the absorbance variation of the films was followed at the visible maxima of the colored isomer (**Figure 3-5, b**). The films were irradiated for 60 s to induce the formation of the transient colored isomer of PhI (MC), confirmed by the increase of the absorbance up to a plateau indicating the achievement of the PSS. At this point (t = 0), the irradiation was stopped and the absorbance decrease at 603 nm was monitored for further 60 s, during which the film was allowed to fade back to the colorless state in the dark**.** The temperature along the process was maintained around 25 ºC by means the air conditioner in the laboratory, since it is well known that the temperature has an important effect in the photochromic fading rates**.**[14]
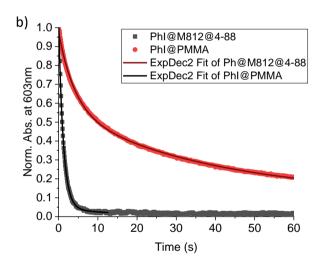
*Figure 3-5: UV-vis spectra (a) and fading kinetics normalized to the absorbance at the PSS (b) of **PhI@PMMA** and **Ph@M812@4-88** films.*

To be able to compare the fading kinetics between the two films, the time-dependent absorbances were normalized to the respective absorption value at the photostationary state (thus fixed to Abs. = 1). The normalized kinetic profiles were then fitted by biexponential decay functions with the general expression noted in **Equation 3-1**. The obtained rate constants (k_1 and k_2) and the half-lifetime ($t_{1/2}$) and three-quarters-lifetime ($t_{3/4}$) of the transient colored species were extrapolated by

35

the fitting curves and are presented in **Table 3-1**. Complete definition of the $t_{1/2}$ and $t_{3/4}$ values, and the method to calculate them is presented in the experimental section (**Section 7.3.4.2**).

Equation 3-1: general expression for a biexponential fading decay function.

$$A_t = A_1 * \exp(- k_1 * t) + A_2 * \exp(- k_2 * t) + Y_0$$

Table 3-1: Half-lifetime ($t_{1/2}$) three-quarters-lifetime ($t_{3/4}$) and biexponential decay fitting constants of PhI dispersed in NEE and PMMA films.

Film	$t_{1/2}$ (s)	$t_{3/4}$ (s)	A1	k_1 (s^{-1})	A2	k_2 (s^{-1})	Y_0
PhI@M812@4-88	0.9	1.8	0.99 ± 0.01	0.85 ± 0.01	0.04 ± 0.03	0.07 ± 12.6	0.01 ± 0.04
PhI@PMMA	9.9	45	0.40 ± 0.00	0.24 ± 0.01	0.46 ± 0.00	0.03 ± 0.01	0.11 ± 0.00

As expected, the fading kinetics of PhI in the NEE film was much faster than in a standard PMMA solid matrix, being the $t_{1/2}$ an order of magnitude smaller. This proved the viability of NEE as approach to achieve solid and transparent materials with fast photochromic performances.

The fitting function for the **PhI@M812@4-88** film only has insignificant contribution from the second pre-exponential decay factor (A_2), which is related to the slow portion of the fading. This indicates that the PhI dye molecules are principally homogenously dissolved in the liquid lipophilic nanodroplets, with low steric hindrance, rather than in the PVA matrix. In contrast, the **PhI@PMMA** film has important contributions from both pre-exponential decay factors and lower fading rate constants, indicating: a) the presence of inhomogeneous dominions of the dye molecules in the PMMA matrix and b). the predominance of rigid PMMA environment in the vicinity of the PhI molecules, which impose a much higher steric hindrance than a liquid solution, slowing the fading kinetics.

Moreover, the obtained lifetimes for the colored isomer of PhI in NEE film was alike to those reported by our group for a bulk M812 liquid solution and to microcapsules-based films (**Figure 3-6**).[2] The small difference on the fading times of this systems (NEE film, M812 bulk solution and capsules based film) was ascribed to temperature differences during the measurements.
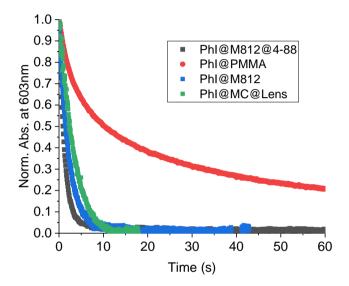
*Figure 3-6: normalized fading process for PhI in bulk M812 solution (**PhI@M812**), in PMMA matrix (**PhI@PMMA**), in microcapsules-based film (**PhI@MC@Lens**)and in NEE film (**PhI@M812@4-88**).*

Figure 3-7 shows a visual comparison of the fading process of the photoactivated PhI dissolved in the NEE film, with a M812 liquid bulk solution (**PhI@M812**), the microcapsules-based acrylate film (**PhI@MC@Lens**) and a PMMA film (**PhI@PMMA**), previously reported by our group.

The **PhI@MC@Lens**, **PhI@M812@PVA** films and the **PhI@M812** bulk solution all fade completely after 5 s, while the PhI@PMMA film is still significantly colored after 40 s. As expected, both encapsulation and NEE strategies provided solid films with liquid-like fast photochromic response. However, the NEE approach clearly yielded a much more transparent film than the obtained with microcapsules.
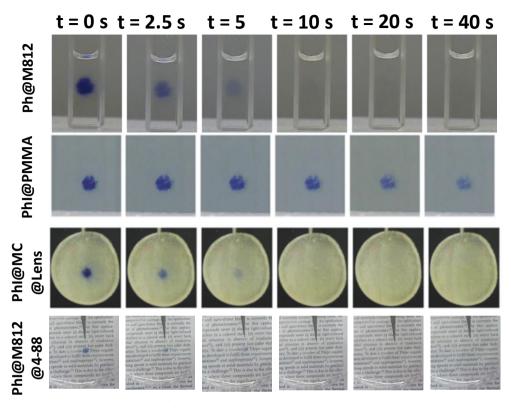
*Figure 3-7: photographs of the fading process for PhI in bulk M812 solution (**PhI@M812**), in PMMA matrix (**PhI@PMMA**), in microcapsules-based film (**PhI@MC@Lens**)and in NEE film (**PhI@M812@4-88**).*

3.2.2 NEE film structure and composition

Once demonstrated the viability of fabrication of transparent and fast responsive photochromic films via NEE, different characterization techniques were used to corroborate the internal structure of the final NEE film.

3.2.2.1 *Confocal fluorescence microscopy*

The structure of the NEE film was investigated through confocal fluorescence microscopy. A NEE film was prepared as described above, but replacing PhI with Nile Red, a fluorescent dye ($\lambda^{em}_{max} \approx 600$ nm), in the organic M812 solution. Sodium fluorescein salt was also added to the aqueous PVA solution ($\lambda^{em}_{max} \approx 550$ nm). These dyes could be detected independently by confocal laser scanning microscopy, as it

has been reported previously.[15] The presence of these fluorescent dyes in the two phases allowed to obtain information in the different steps of the film preparation (**Figure 3-8**).
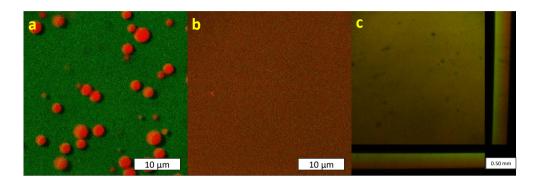
Figure 3-8: confocal laser scanning microscopy of stained preemulsion (a), ultrasonicated nanoemulsion (b), and dried NEE film (c).

In the preemulsion, discrete red oil droplets of size between 1 and 6 µm could be observed dispersed in the green stained aqueous continuous phase (**Figure 3-8, a**). However, once the ultrasonic irradiation was performed to achieve the nanoemulsion, no discrete structures could be detected and only a continuous mixture of green and red pixels was observed (**Figure 3-8, b**). The dilution of the nanoemulsion did not provide any improvement in the image resolution, but only reduced the fluorescent signal. This suggests that the average size of the oil nanodroplets is below the resolution limit of the used equipment (around 200 nm), and that the size distribution of the nanodroplets of the nanoemulsion is narrow and no aggregated or coalesced droplets formed. This is in agreement with the droplet size distribution measured by DLS in (**Figure 3-3**).

Similar results were obtained by imaging the dried NEE film (**Figure 3-8, c**), as no discrete red structures could be observed across the film, indicating that the lipophilic nanodroplets are not coalesced or aggregated to form structures above the detection limit of the equipment. Several dark regions were observed in the film area, though, likely coming from microscopic air bubbles entrapped in the matrix,

dust and/or other contaminants deposited on the film surface during the drying process.

The tomography of the NEE film also revealed a gradient of the red fluorescent signal along the axis perpendicular respect to the film plane: the less intense signal was measured at the bottom surface of the film, (in contact with the polystyrene Petri plate substrate) while the highest intensity was observed at the film upper surface (air-film interface) (**Figure 3-8, c, lateral bar**). This signal variation along the film height was associated to a gradient in the nanodroplets concentration, which suggests flocculation of the nanodroplets during the slow drying process (at room temperature) favored by the lower density of the organic M812 solution compared to the increasingly concentrated PVA aqueous solution. From this result it was suggested that the drying process of the NEE films should be carried inside a closed oven at 40 °C, to increase the evaporation rate and reduce contamination.

Even though this experiment provided insightful information, the presence and the distribution of the lipophilic nanodroplets could not be confirmed by direct fluorescent imaging, mainly because of the insufficient resolution of the technique.

3.2.2.2   *Scanning electron microscopy.*

The structure of NEE films was investigated by observing the surface and cross-section of the films by scanning electron microscopy (SEM), since this technique has a better resolution limit than confocal microscopy (around 20 nm). For these experiments new NEE films were prepared as above, using PhI as dye.

The initial attempts did not yield clear images of the nanodroplets, though. Since the PVA matrix of the NEE films has very low charge conductivity, the electron beam produced built up electrical charge and heat, inducing significant damage to the film surface and, blurring the image (**Figure 3-9, a**). Sputtering a platinum coating improved to a certain degree the sample conductivity and resistance to the electron beam, but no surface motives were observed at the range of sizes the nanodroplets

were expected to be (**Figure 3-9, b**). Upon observation of the film section, it was corroborated that the thickness was about 150 µm. Moreover, it was realized that the cutting techniques used to prepare the sample (scissors or cutters), induced significant deformation of the film (**Figure 3-9, c**), preventing the visualization of the real nanoscopic structure of the section.
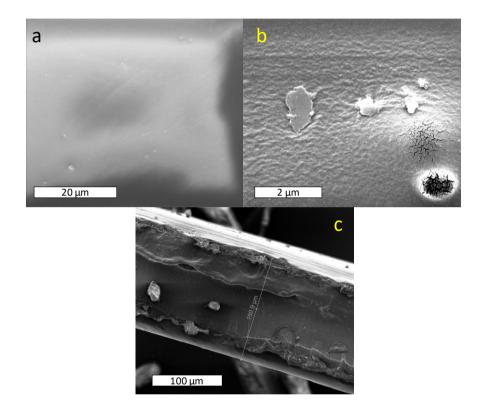
Figure 3-9: SEM images of the non-sputtered NEE film (a), platinum coated NEE film surface (b) and cross-section of NEE film cut with scissors (c).

Taking this into account, improved imaging of the cross-section was achieved by fracturing the NEE films after freezing the sample in liquid nitrogen (avoiding deformation). In this way, roughness and pores at the nanoscale (20-70 nm) could be observed in the interior of cracks and grooves formed in the film, suggesting the presence of nanocavities in the interior of the NEE film (**Figure 3-10**). Even though, the PVA 4-88 matrix was still too sensitive to the electron beam to achieve a clear

image and the attempts to stablish the internal structure of NEE films were interrupted at this point of the research.
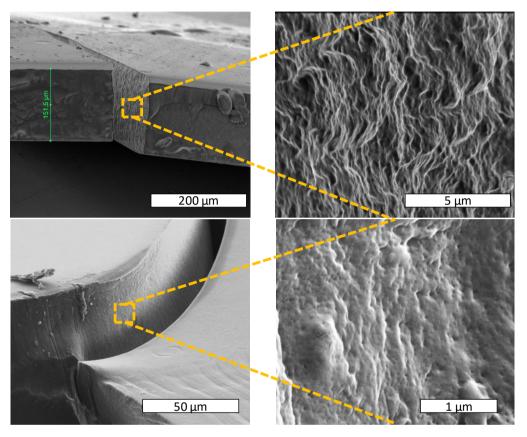
Figure 3-10: SEM imaging of cryo-fractured NEE films.

Finally, clear images of the interior structure and the nanocavities of the NEE films were successfully obtained when more resilient grades of PVA were explored in a later stage of this work, presented in more details in the **Section 4.2**, and applying the learned improved measuring conditions explained above. This films were made from:

a) PVA matrix with higher molecular weight and was cross-linked with glutaraldehyde (**Rev.PP@M812@XL40-88**, **Figure 3-10, a**).

b) PVA matrix with higher hydrolysis degree (**Rev.PP@M812@10-98**, **Figure 3-10, b**).

In both cases, the photochromic dye Reversacol Palatinate Purple (**Rev.PP**) was used as dye instead of PhI.
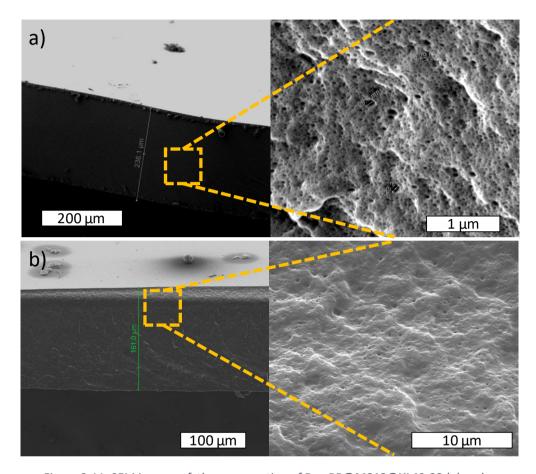
*Figure 3-11: SEM images of the cross-section of **Rev.PP@M812@XL40-88** (a) and **Rev.PP@M812@10-98** (b).*

The surface and the cross-section of this NEE film presented a plurality of nanocavities homogeneously distributed, indicating the position that the lipophilic nanodroplets should have occupied inside the NEE film before they were removed during the cryo-fracture preparation process.

The size distribution of the nanocavities is in agreement to the DLS measurements of the nanoemulsion of each sample, ranging from 50 nm to 150 nm, with an average around 90 nm, for **Rev.PP@M812@XL40-88**, and from 100 nm to 500 nm, with an average around 200 nm for **Rev.PP@M812@10-98**, further

indicating the former presence of the lipophilic nanodroplets inside these cavities. The cavities do not present hints of interconnectivity between them or aggregation of the nanodroplets.

3.2.2.3 Thermal analysis of NEE films.

To assess the mechanical and thermal stability of the NEE films, differential scanning calorimetry (**DSC**) and thermo-gravimetrical analysis (**TGA**) were performed to determine the glass transition temperature (T_g), melting temperature (T_m)the water content and l decomposition temperature (T_d) of the NEE films.

The results were compared to the crystalline form of PVA, which is how is provided, and to a plain PVA film prepared by solution-casting process identical to the NEE film casting, but without incorporating the lipophilic nanodroplets dispersed in it (**Figure 3-12** and **Table 3-2**).
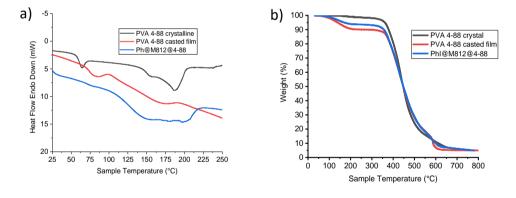
Figure 3-12: DSC (A) and TGA (B) analysis of PVA 4-88 in crystalline form (black), a solution-casted film (red) and as NEE film (blue).

Table 3-2: DSC and TGA results

Sample	T_g (°C)	T_m (°C)	T_d (°C)	Water Content (wt. %)
Crystalline PVA 4-88	56.8	150-200	360	1
Solution-casted PVA 4-88 film	73.6	120-190	360	10
PhI@M812@PVA 4-88 film	71.0	120-200	360	6

The water content of the NEE film was found to be of 6 wt.% and the T_g was of 71 °C. These results are similar to those observed for the solution-casted PVA film that did not contain nanodroplets dispersed in it (10 wt.% of water, T_g = 73.6 °C). This indicates that the integrity of the film is not compromised by the presence of the nanodroplets at temperatures below the T_m of PVA.

From the DSC analysis it was also observed a widening of the band related with the PVA melting, between 120 and 200 °C, with respect to the crystalline PVA and the plain PVA film, indicating that the lipophilic solvent acts as plasticizer of the PVA matrix at these high temperatures. Moreover, thermal degradation and volatilization only started at 360 °C in all the studied samples (with less than 5% of solid residue after 700 °C). These results suggest that the droplet-based structure may be maintained in the films up to 120 °C and that the thermal decomposition only occurs after heating above 360 °C.

3.3   Universality of the emulsion entrapment technique

3.3.1   Substitution of the dye

After demonstrating the feasibility of NEE films as transparent fast responsive photochromic materials using the model photochromic dye PhI, a screening across different commercial dyes was made. The aim of this test was threefold:

a) To proof the universality of the NEE technique for T-type photochromic dyes other than PhI.

b) To improve the color development of the NEE films as they are exposed to sunlight, since PhI has little absorption change when irradiated.

c) Achieve NEE films could provide different colors after UV irradiation, that could be more attractive to different applications.

Seven different commercial dyes provided by Vivimed Labs under the branding name Reversacol™ were tested to demonstrate its applicability to different product designs. Even though the molecular structure of this dyes is not publicly disclosed to customers, it is known that they are derivatives belonging to the spirooxazines and naphthopyrans families, which are T-type photochromes, making them good candidates to be used with our technology.

NEE and PMMA films with these dyes were prepared and characterized as above, described in detail in the experimental **Chapter 7.1**. When irradiating with UV light, the resulting films displayed the color according to the dye used. No color difference was observed between the PMMA and the NEE films (no solvatochromism).

The visual aspect of the NEE films in the dark and exposed to sunlight is showed in the digital photographs of **Figure 3-13**. In the colored films it is specified the commercial name of the corresponding dye, while the numbers indicated in the unactivated films are related to the time required by the films to fade completely. The comparison of fading half-lifetimes ($t_{1/2}$) of the photoactivated colored form of the dyes is presented in **Table 3-3**. For very slow fading kinetics, the $t_{3/4}$ value was extrapolated form the fitting function.

Remarkably, for all the commercial dyes tested, the $t_{1/2}$ and $t_{3/4}$ fading times in NEE films were at least one order of magnitude lower than in PMMA proving the universality of the nanoemulsion entrapment technique and the versatility to produce fast responsive photochromic products of different colors with T-type photochromic dyes.
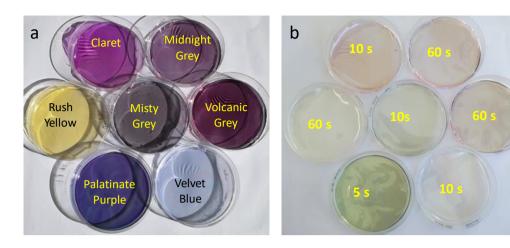
Figure 3-13: photographs of the NEE films prepared with different commercial dyes, activated by sun-light (a) and in shades (b)

Remarkably, for all the commercial dyes tested, the $t_{1/2}$ and $t_{3/4}$ fading times in NEE films were at least one order of magnitude lower than in PMMA proving the universality of the nanoemulsion entrapment technique and the versatility to produce fast responsive photochromic products of different colors with T-type photochromic dyes.

Table 3-3: calculated $t_{1/2}$ and $t_{3/4}$ kinetics of commercial dyes in NEE films and PMMA films.

Reversacol™ dye branding name.	NEE		PMMA	
	$t_{1/2}$ (s)	$t_{3/4}$ (s)	$t_{1/2}$ (s)	$t_{3/4}$ (s)
Palatinate Purple	1.4	2.5	109	342
Claret	3.6	7.6	120	607
Midnight Grey	11	29	1650 [a]	3050 [a]
Volcanic Grey	12	29	1800 [a]	3200 [a]
Graphite	73	216	8000 [a]	17000 [a]
Misty Grey	2.6	6.0	293	1400 [a]
Velvet Blue	2.6	5.3	40	146
Rush Yellow	8.9	46	38	382

a) extrapolated from fitted function

Moreover, the NEE films with Reversacol™ Palatinate Purple (**Rev.PP**), Reversacol™ Claret (**Rev.Claret**) and Reversacol™ Misty Grey (**Rev.Misty**), took less than 10 seconds to fade completely, which means these films were two orders of magnitude faster respect to the PMMA films. Despite the similar fading times of these films to that made of PhI, these shown a much higher photostationary color intensity (**Figure 3-14**). For this reason, and due to their easy accessibility, Rev.PP, Rev.Claret and Rev.Misty were selected over PhI as dyes for some of the future studies and optimization of the NEE films formulation.
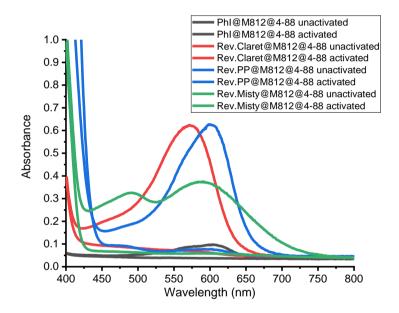
Figure 3-14: UV-Vis spectra of NEE films containing PhI (black), Rev.Claret (red), Rev.PP (blue) and Rev.Misty (green), in their unactivated and at the photostationary state.

3.3.2 Effect of the hydrophobic oil

After testing the universality of the NEE technique with different dyes, the effect of changing the lipophilic oil solvent was explored. Rev.PP was selected as dye for this study since, even though its molecular structure is not of public domain, its kinetic response is similar to that of PhI and the intensity of the photoinduced coloration is much superior.

Rev.PP was dissolved in 14 different oils of different polarities and viscosities. These oil solutions were used to prepare the corresponding NEE films whose photochromic kinetic responses were measured as previously explained. The list of oils used in the NEE films and the $t_{1/2}$ and $t_{3/4}$ obtained from the fitting functions of the normalized fading kinetics are summarized in **Table 3-4**, sorted the $t_{3/4}$ fading time. The fitting functions of the fading processes and the visual aspect of this 14 NEE film are shown in **Figure 3-15** and **Figure 3-16** respectively.

Table 3-4: calculated $t_{1/2}$ and $t_{3/4}$ of NEE films containing Rev.PP dissolved in different oils.

Code	Name	Type	$t_{1/2}$ (s)	$t_{3/4}$ (s)
DEP	Diethyl phthalate	Aromatic ester	0.8	1.6
HD	Hexadecane	Alkane	1.3	2.6
SiAR20	Polyphenyl-methylsiloxane ≈ 20 mPa.s	Silicon oil	1.6	3.3
M829	Miglyol® 829	Triglyceride	1.9	3.6
M812	Miglyol® 812	Triglyceride	2.2	4.2
M840	Miglyol® 840	Triglyceride	3.2	4.6
DISDAd	Diisodecyl adipate	Alkylic ester	2.3	4.6
SiAP1000	Polyphenyl-methylsiloxane ≈ 1000 mPa.s	Silicon oil	2.4	4.8
PEG2EHt	Poly(ethylene glycol) bis(2-ethylhexanoate)	PEG/alkylic ester	2.6	5.1
BEHSb	Bis(2-ethylhexyl) sebacate	Alkane ester	2.7	5.3
DOT	Dioctyl terephthalate	Aromatic ester	4.8	9.6
HxBz	Hexylbenzene	Alkylic aromatic	5.0	11
3Ph3Ch	3-Phenyl-3-cyclohexane	Alkylic aromatic	7.8	16
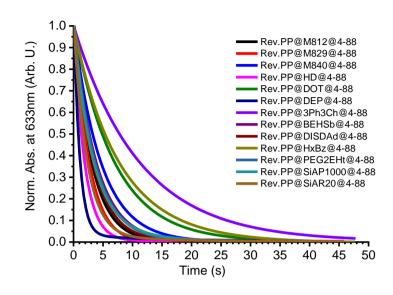
Figure 3-15: fitting functions of the normalized fading process of NEE films containing Rev.PP dissolved in different oils.
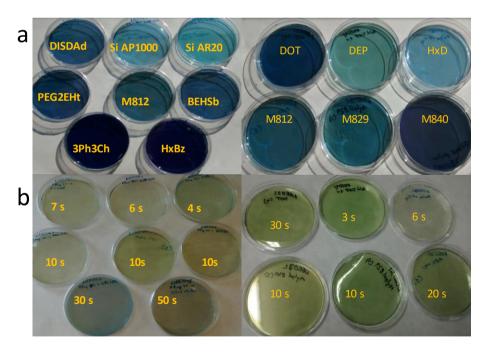
Figure 3-16: photographs of NEE films containing Rev.PP dissolved in different oils , activated by sun-light (a) and in shades (b).

The photoactivated color intensity and the fading rate of the NEE films were very dependent on the type of oil. As it was expected,[16] the NEE films containing oils that induced a faster fading rates (DEP, HD and SiAR20) also displayed the lowest colorability. In the same way, NEE films prepared from oil solutions that induced a slower fadings (DOT, HxBz and 3Ph3Ch) showed stronger photocoloration when irradiated with sunlight.

A clear correlation between the solvent type and the fading times could not be inferred, although relevant conclusion could be extracted from this experiment. Photochromic fading kinetics are known to be affected by several factors of the solvents, such as polarity, viscosity, pKa and the solubility of each of the isomers.

The viscosity effect could be appreciated by comparing the fading kinetics of the NEE films prepared from Rev.PP dissolved in the two silicon oils. Since these oils have the same chemical units, the difference in fading rate can be attributed only to viscosity. The silicon oil with the lowest viscosity (SiAR20, ≈ 20 mPa.s) induced faster fading time than the more viscous one (SiAP1000, ≈ 1000 mPa.s), since the second provides more impediment to the isomerization process,[17] similarly to the stearic hindrance related to the matrix effect provided by rigid polymer media.

The effect of the solvent polarity is more complex to define. The MC form of the spirooxacines might be stabilized by polar solvents (protic and non-protic), reducing the rate of the ring-closure reaction. However, the extent of the MC stabilization depends on the functional groups of the photochromic dye and the type of interactions that the molecule can do with the media (hydrogen bonding, dipole interaction, etc). [18] Therefore, without knowing the structure of this dye (which is not publicly known) it is not possible to reason the trend of the obtained fading kinetics. Furthermore, the tendency observed for Rev.PP may or may not apply to other dyes, for which new trend investigation would be needed.

However, this experiment did prove that the fading kinetics of the photochromic dyes in NEE films is dependent on the organic oil entrapped in the PVA matrix. This opens the possibility of fine tuning the fading kinetics of NEE films to match desired applications, or to tune the kinetics of different dyes to match their fading rates.

3.3.3   Effect of the film-forming, water soluble polymer

After exploring the universality of the NEE technique with different dyes and lipophilic oils, the effect of changing the film-forming polymer was explored. NEE films with different grades of PVA were also explored in a later state of this PhD project, and are presented at **Section 0**, but in this chapter, only attempts to produce transparent NEE films with water soluble polymers other than PVA are reported.

The initial approach was to substitute PVA by other film forming water soluble polymers, like polyacrylamide (**PAM**) and hydroxyethyl cellulose (**HECell**). Two aqueous solutions of this polymers were prepared at the maximum concentration achievable (3 wt.% and 5 wt.% respectively) and used as the continuous phase for the nanoemulsification process.

These solutions, however, had less stabilizing properties than the PVA 4-88 solution, and 0.1 wt.% of the ionic surfactant sodium dodecyl sulfate (SDS) had to be added. After 10 minutes of ultrasonic irradiation, strong bluish coloration was observed due to the Tyndall effect, indicating the formation of the nanodroplets, but clear transparency of the nanoemulsion was not achieved. This nanoemulsions were then casted on polystyrene Petri plates and allowed to dry at 40 °C overnight.

DLS analysis of the nanodroplets size, the visual aspect and the UV-vis spectra of the films obtained are presented at **Figure 3-17**. Though both the emulsions had droplets in the nanometric scale, neither of the obtained films turned out transparent after the water was evaporated, likely due to coalescence of the

nanodroplets. This experiment shows that PVA is better in stabilizing the oil nanodroplets while the film is formed.
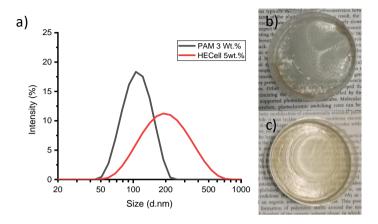
Figure 3-17: DLS analysis (a) and photographs of NEE films prepared with PAM (black, b) and HECell (Red, c).

3.4   Effect of temperature on the photochromic performances of the NEE films

T-type photochromic dyes are inherently sensitive to temperature.[14,19] This means that the temperature variation occurring during the same day, or in different seasons and geographical points, might have important consequences on the final photochromic properties of the devices.

Therefore, the photochromic properties of the NEE films at different temperatures needed to be investigated. A temperature-controlled study of the NEE films was carried out by using a custom film holed holder. This holder consisted of two copper plates in which 3 sapphire windows of 1 cm of diameter were integrated. The copper plates were connected to a thermostatic batch to control their temperature (**Figure 3-18**).
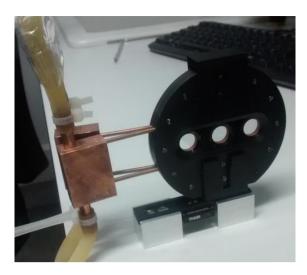
Figure 3-18: Custom film holder for temperature controlled TAS measurements.

The photostationary absorbance and the fading kinetics of a NEE film containing Rev.PP were measured at different temperatures, using the unactivated form of the NEE film as 100%T reference (**Figure 3-19, a**). After measuring the absorption spectra at each temperature, the excitation light source was turn off and the fading kinetics recorded as well (**Figure 3-20, a**).

The reaction rate could not be calculated, as neither the molecular weight of Rev.PP nor the molar attenuation coefficient of its colored form are known. However, an inverse correlation between the temperature and both PSS absorbance and the $t_{1/2}$ was obtained (**Figure 3-19, b** and **Figure 3-20, b**).

As expected, the $t_{1/2}$ of the NEE film decreased with the temperature and, as consequence, the maximum absorbance achieved at the PSS diminished as well This supposes an important detriment for applications expected to withstand warm temperatures, like sunglasses, usually worn at summer hot days. On the other hand, lowering the temperature slows the fading rate and increases the maximum absorbance at the photoequilibrium state. This is also a feature to take into account when designing NEE films to be applied on devices expected to withstand cold climates, like skiing glasses.
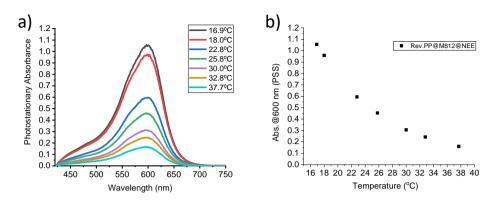
Figure 3-19: absorbance spectra (a) and absorbance at λ$_{max}$ = 600 nm (b) of Rev.PP@M812@4-88 at different temperatures at the PSS.
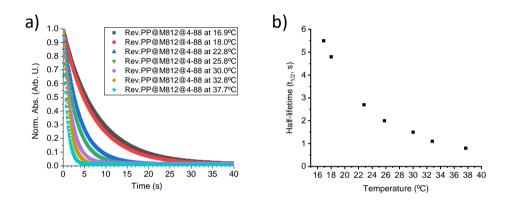
Figure 3-20: fading profiles (a) and Half-lifetimes (t$_{1/2}$) (b) of Rev.PP@M812@4-88 at different temperatures at the PSS.

3.5 Preliminary fatigue study

As a first approach to assess the fatigue resistance, a NEE film (Rev.PP@M812@4-88) was subjected to seven cycles of photoactivation and fading in the dark. The UV-vis absorption spectra of the NEE film were recorded for each cycle at the PSS and after complete color fading, using the custom set-up explained at **Section 3.2.1**.

The evolution of the absorption at λ$_{max}$ = 600 nm is presented at **Figure 3-21**. An increase of the absorbance of the film at the PSS along the cycles could indicate migration of the Rev.PP dye molecules to the more rigid and polar PVA matrix (which

would increase the MC lifetime), while a decrease of absorbance could indicate photodegradation of the dye. A possible increase of the absorption of the unactivated film would indicate a build-up of degradation byproducts, aggregation of the nanoparticles or microscopic crystalline dye precipitation.

No significant changes of absorption were observed at the PSS nor in the faded state, indicating that the photochromic transition is fully reversible and the film stable to fatigue at least during the short light exposures (60 s) of each cycle. An additional, more demanding fatigue test of accelerated aging by UV light exposure (**QUV** test) was performed by the end of this doctoral research (**Section 4.4**).
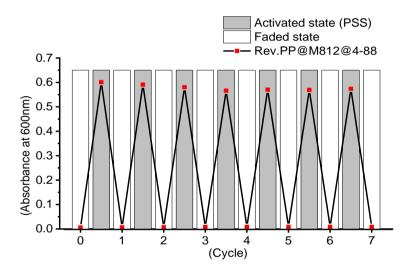
Figure 3-21: Evolution of PSS and faded absorption at λ_{max} after 7 cycles.

3.6   Time stability of the nanoemulsion

Though nanoemulsions are kinetically stable, they are thermodynamically unstable, and therefore their properties inevitably change upon long periods of time.[20] Taking this into account, the effect of aging and storage of the photochromic nanoemulsion on the quality of the NEE film was studied, as this could give insights for future mass production.

For this, a 200 g batch of nanoemulsion was prepared using Rev.PP as photochromic dye, M812 as oil and PVA 4-88 as film forming polymer. The ultrasonic probe was changed to a 25.4 mm diameter high gain probe, to better emulsify the larger volume of this synthesis batch. The vibration amplitude was also increased to 100% and the sonication time extended up to 70 minutes to achieve similar droplet size distribution as described for regular synthesis batches. The emulsion was kept in an ice/water bath during the emulsification process to mitigate heat build-up. The so produced nanoemulsion was transferred to a close lid container and stored at room temperature.

Three films were prepared by casting 10 grams of this emulsion in a polystyrene Petri plates. One of these films was obtained casting the nanoemulsion immediately after its preparation (0-Months). The second and the third films were prepared after one (1-Month) and two months (2-Months) of aging storage of the nanoemulsion, respectively. The visual aspect and the UV-vis transmittance spectra of these films are presented in **Figure 3-22** and **Figure 3-23** respectively.
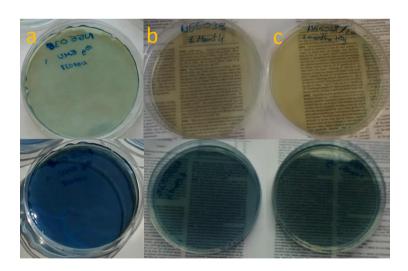
Figure 3-22: digital photographs of unactivated and photoactivated Rev.PP@M812@4-88 casted immediatedly after preparation (a) after 1 month of aging (b) and after 2 months of aging (c).
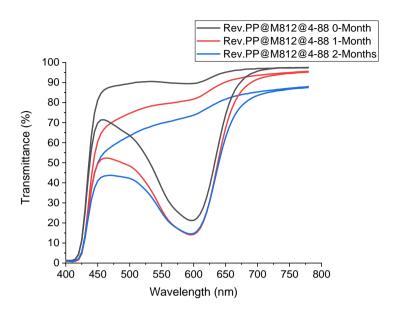
Figure 3-23: UV-vis transmittance spectra of the unactivated and photoactivated forms of Rev.PP@M812@4-88, casted immediately after preparation (a) after 1 month of aging (b) and after 2 months of aging (c).

It was found that the films obtained from aged nanoemulsion consistently decreased their unactivated transmittance. Moreover, the transmittance of the films decreased unevenly from about 90 % transmittance across the visible range, to about 55 % at λ = 450 nm wavelength and 87 % at λ = 750 nm for the film obtained from the 2-month stored nanoemulsion. Also the PSS transmittance decreased by 6% after the two month of aging (**Table 3-5**).

Table 3-5: transmittance of films casted from aged nanoemulsion at different wavelengths, in the unactivated form and at the PSS state.

Nanoemulsion aging time	Unactivated			Activated to PSS		
	T% at 450 nm	T% at 600 nm	T% at 750 nm	T% at 500 nm	T% at 600 nm	T% at 700 nm
0-Month	89.5 %	89.5 %	97.2 %	63.6 %	21.3 %	97.2 %
1-Month	62.1 %	81.7 %	94.5 %	48.4 %	14.8 %	94.5 %
2-Months	54.7 %	73.7 %	86.7 %	42.2 %	14.8 %	86.7 %

This overall decrease of the transmittance in the visible region, and predominantly at the shorter wavelengths, recalls the typical light scattering profile given by dispersed nanoparticles of diameter of the range of the visible wavelength (Tyndall effect)[21,22] which induce larger light scattering at shorter wavelengths. This is suggesting that the droplets dispersed in the stored nanoemulsions are slowly aggregating and possibly coalescing upon time, increasing the scattering of the films obtained from these.

The fading kinetics of the two aged NEE films were almost identical to that of the initial film. The little variation could be also ascribed to small differences in the room temperature when the measurements were performed (**Figure 3-24**).

From this experiment, it was concluded that the casting of the NEE films should be done as soon as possible after the emulsification process, discouraging the long term storage of the nanoemulsions and the on-demand casting of the NEE films.
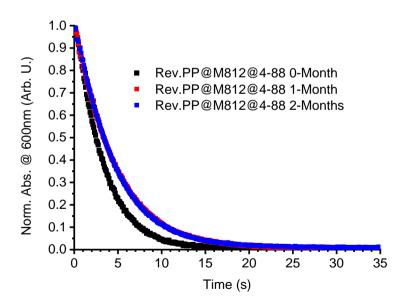
Figure 3-24: normalized fading kinetics of NEE films casted from nanoemulsion immediately after (black), after one month (red), and after 2 months of the nanoemulsion preparation (blue).

3.7   Photochromic film recyclability

The recycling of NEE films was investigated for its relevance in the mass production. The objective was to determine the feasibility of preparing large sheets of the NEE film, from which the desired parts could be cut and integrated in the final product. The exceeding portions could be recycled by dissolving them in water and recasting the resulting nanoemulsion.

Two groups of three NEE films were prepared as described in section 3.1, but using Rev.Misty as photochromic dye at 1 wt.% concentration. These groups were labeled as **Mag-C1** and **US-C1**, the code C1 indicates the first casting cycle. The droplet size of each emulsion sample was measured by DLS. The UV-vis spectra and the fading times of the casted films samples are presented in **Table 3-6**. The average values of all the measured parameters for Mag-C1 and US-C1 films were almost identical and within the standard error, and therefore were used as reference to assess the effect of dissolving and re-casting the films.

The group labeled as Mag-C1 were then dissolved in distilled water by magnetically stirring and the nanoemulsions (formed directly upon film dissolution) were re-casted into a polystyrene Petri plate. These three films were labeled as **Mag-C2**. The other three films labeled as US-C1 were also dissolved in H_2O by magnetic stirring, but the obtained nanoemulsions were subjected to an ultrasonication step before being re-casting the film, and were labeled as **US-C2**. These films were characterized as done in the first cycle.

This process was repeated for a third casting cycle, generating **Mag-C3** and **US-C3** films. The characterization results of all these films are summarized in **Table 3-6**, including the standard deviation (**St.Dv.**) calculated from the values of the replicates of each type of film. The visual aspect of samples of these films is presented in

. The UV-vis transmittance spectra of these film are reported at the annexes (**Figure 8-1**).

Table 3-6: values of droplet size and photochromic performance of the NEE films after three casting cycles.

Films	Z-average (nm) / St. Dv.	Unactivated T% @450 nm (%) / St. Dv.	Activated T% @450 nm (%) / St. Dv.	$t_{1/2}$ (s) / St. Dv.	$t_{3/4}$ (s) / St. Dv.
Mag-C1	100 / 10	76.6 / 3.7	64.5 / 4.9	3.5 / 0.1	7.4 / 0.4
Mag-C2	149 / 23	76.6 / 1.7	63.3 / 1.6	3.9 / 0.3	8.8 / 0.7
Mag-C3	122 / 7.3	73.5 / 1.5	61.2 / 1.4	3.7 / 0.	8.7
US_C1	110 / 6.2	80.0 / 2.8	65.8 / 2.3	3.2 / 0.5	7.6 / 0.2
US_C2	131 / 31	81.8 / 1.7	65.8 / 4.4	4.2 / 0.2	9.3 / 0.5
US_C3	121 / 10	74.7 / 1.5	62.2 / 0.8	4.0	9.5
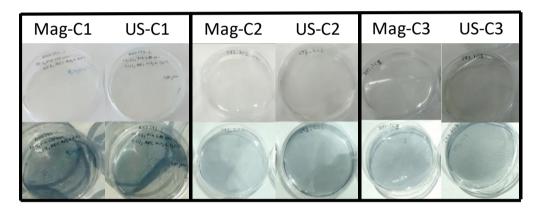
Figure 3-25: digital photographs of NEE films upon recasting cycles.

First of all, the average droplet size (Z-average) of the re-dissolved solutions increased approximately 50 nm for the non-sonicated solutions (Mag-C2) and approximately 20 nm for the sonicated ones (UC-C2) respect to the C1 nanoemulsions, and the standard deviation increased too. However, the films obtained from the two sets of emulsions were optically transparent and well formed, with no visible defects. The average results of the photochromic performances of the C1 NEE films and the C2 NEE films are similar and within the standard error deviation.

After the second redissolution (C3), the Z-average of the nanoemulsions was 10 nm larger than of the initial one. Moreover, there was not a clear difference between the droplet size of Mag-C3 and US-C3, meaning that there is not a clear effect of adding the sonication step between the film dissolution and the casting to the measured parameters of this study. However, a slight decrease of the shorter wavelengths transmittance was also observed, for both Mag-C3 and US-C3 (**Figure 3-26**), accompanied by slight slower fading kinetics. This suggest some coalescence of the nanodroplets along the recasting process.
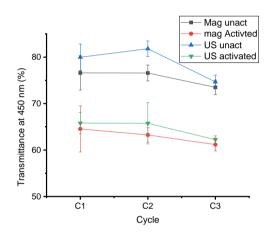
Figure 3-26: evolution of the transmittance values at 450 nm upon recasting cycles.

This results may be of interest when considering the industrial process of production in large scale, meaning that it is possible to produce large sheets of NEE film, cut the desired portions from them and recycle the residual parts. Adding a sonication step before casting the dissolved films gave little evidence of droplet size reduction, and the transmittance of the films was not different.

However, it was observed a slight decrease of transmittance at shorter wavelengths in the visible range after the third casting for some of the NEE films, indicating that the feasibility of reusing the residual pieces may be limited to only one redisolution and recasting cycle, though it may be possible to minimize this loss of transmittance by improving the redisolution and the sonication conditions.

3.8   Conclusions

Along this chapter, the viability of the NEE technology to achieve transparent fast fading photochromic films has been proven. Solid NEE films with high visual transparency and liquid-like fading kinetics were obtained by:

i)   dispersing a lipophilic dye solution into an aqueous PVA 4-88 solution though ultrasonic irradiation

ii)   acasting the resulting nanoemulsion on a polystyrene substrate and allowing the water to evaporate.

The internal structure of these films was corroborated by scanning electron microscopy. A plurality of nanocavities at the cross-section of the NEE films were detected when using the cryo-fracture technique that indicate the location of the nanodroplets in the NEE film before the fracture.

The universality of the technique was subsequently explored, substituting the photochromic dyes, the oil solvent, and the polymeric matrix. Different photoinduced colorations could be obtained from different dyes. The fading kinetics of these dyes in NEE films were an order of magnitude faster than those of the solid solutions of PMMA used as control. Various oils of different chemical nature were successfully emulsified and entrapped into the NEE films. The fading kinetics of the photochromic dye could be finely tuned by selecting the appropriate lipophilic solvents. Two water soluble polymers (HECell and PAM) were also tested as film forming polymers, but were unable to produce visually clear NEE films with the tested preparation conditions.

Finally, the robustness of this method was studied. Dependency of the fading kinetics and the temperature was observer, which in turn affected PSS maximum absorbance of the NEE film. Good reversibility and fatigue resistance was observed after 7 cycles of photoactivation (up to PSS) and fading in the dark. The droplet size of the nanoemulsion increased after 1 month of storage. However, recycling already

formed NEE films to obtain transparent films that retain the same optical properties was possible, by simply dissolving them into distilled water and re-casting the resulting solution into polystyrene Petri plates.
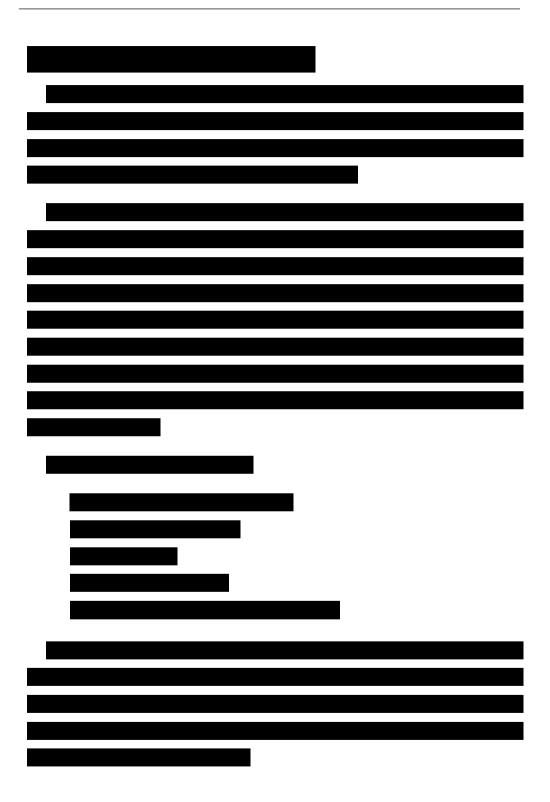
3.9   References
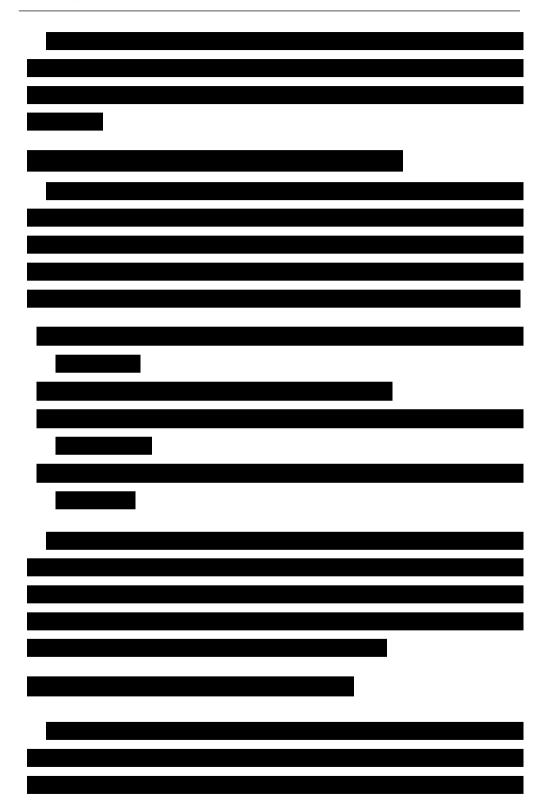
[1]   J. Hernando, C. Roscini, N. Vázquez-Mera, D. Ruiz-Molina, *Coating With Photochromic Properties, Method For Producing Said Coating And Use Thereof Applicable To Optical Articles And Glazed Surfaces*, **2015**, US20150024126A1.

[2]   N. Vázquez-Mera, C. Roscini, J. Hernando, D. Ruiz-Molina, *Adv. Opt. Mater.* **2013**, *1*, 631.

[3]   C. Roscini, H. Torres-Pierna, D. Ruiz-Molina, *Nanoemulsion optical materals*, **2017**, US20170166806A1.

[4]   H. Torres-Pierna, C. Roscini, J. Hernando Campos, *Fast Responsive Photochromic Materials Based on Polymeric Nanoparticles*, Master Thesis, Universitat Autònoma de Barcelona, **2014**.

[5]   S. Long, S. Bi, Y. Liao, Z. Xue, X. Xie, *Macromol. Rapid Commun.* **2014**, *35*, 741.

[6]   H. Torres-Pierna, C. Roscini, A. Vlasceanu, S. L. Broman, M. Jevric, M. Cacciarini, M. B. Nielsen, *Dyes Pigm.* **2017**, *145*, 359.

[7]   H. Bouas-Laurent, H. Dürr, *Pure Appl. Chem.* **2001**, *73*, 639.

[8]   N. Sadurní, C. Solans, N. Azemar, M. J. García-Celma, *Eur. J. Pharm. Sci.* **2005**, *26*, 438.

[9]   M. Mishra, Handbook of Encapsulation and Controlled Release, CRC Press, **2015**.

[10]   G. Le Bars, S. Dion, B. Gauthier, S. Mhedhbi, G. Pohlmeyer-Esch, P. Comby, N. Vivan, B. Ruty, *Regul. Toxicol. Pharmacol.* **2015**, *73*, 930.

[11]   Sasol, Excipients for Pharmaceuticals, can be found under http://www.sasoltechdata.com/MarketingBrochures/Excipients_Pharmaceuticals.pdf, last access: November **2019**

[12]   Clariant, Mowiol Supplier Literature, can be found under https://mafiadoc.com/mowiol-clariant_5c27db7a097c47c0648b45e7.html, last access: November **2019**.
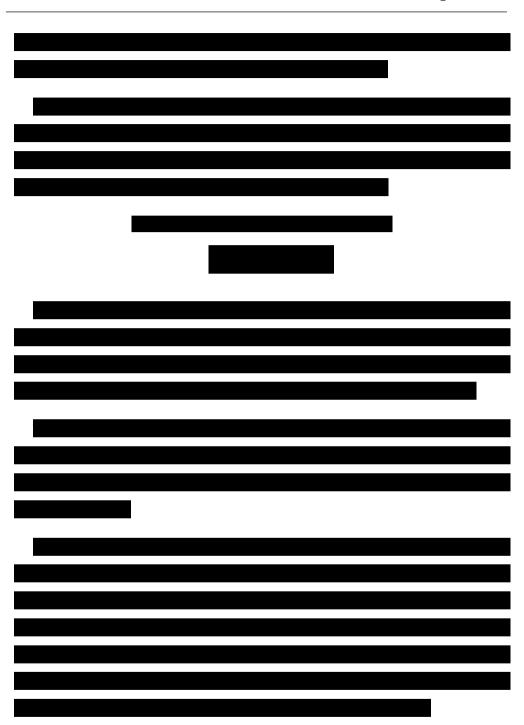
[13] J. W. Gentry, *J. Aerosol Sci.* **1997**, 28, 1365.

[14] F. Ortica, *Dyes Pigm.* **2012**, *92*, 807.

[15] A. R. Abhyankar, D. M. Mulvihill, M. A. E. Auty, *Food Hydrocoll.* **2011**, *25*, 275.

[16] G. Favaro, V. Malatesta, U. Mazzucato, G. Ottavi, A. Romani, *J. Photochem. Photobiol., A.* **1995**, *87*, 235.

[17] A. P. Periyasamy, M. Vikova, M. Vik, *Text. Prog.* **2017**, *49*, 53.

[18] S. Minkovska, B. Jeliazkova, E. Borisova, L. Avramov, T. Deligeorgiev, *J. Photochem. Photobiol., A* **2004**, *163*, 121.

[19] L. Ouyang, H. Huang, Y. Tian, W. Peng, H. Sun, W. Jiang, *Color. Technol.* **2016**, *132*, 238.

[20] M. E. Helgeson, Curr. Opin. *Colloid Interface Sci.* **2016**, *25*, 39.

[21] D. W. Hahn, Light Scattering Theory, can be found under http://plaza.ufl.edu/dwhahn/Rayleigh%20and%20Mie%20Light%20Scattering.pdf, last access: November **2019**.

[22] A. J. Cox, A. J. DeWeerd, J. Linden, *Am. J. Phys.* **2002**, *70*, 620.
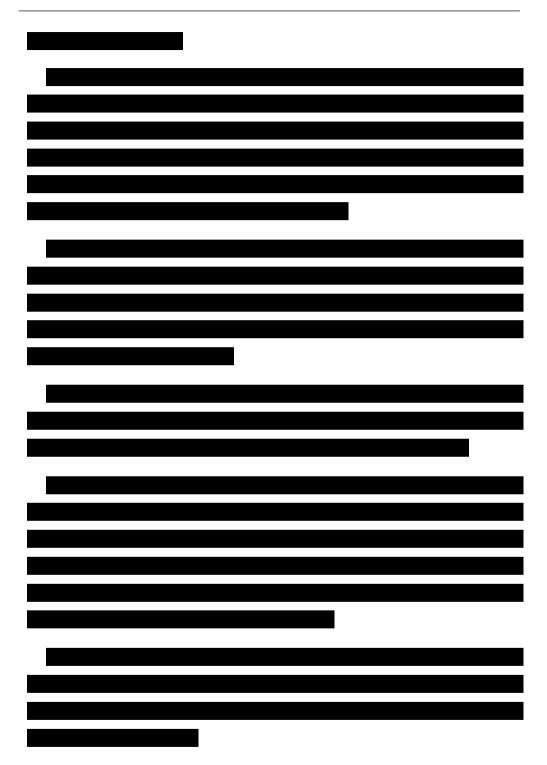
Chapter 4

Towards commercial products

73

██

██

██

██

████████████

████████████████████	███████████████	███████████████
██████████	█	█	█	██	██	█
████████████	█	█	█	█	█	█
██████████████	█	█	█	██	█	█
████████████████	█	█	█	█	█	█

██

██

██

██

██

██

██

██

██

██████████████████████████████

██

██

██

██

██

█████████████████████████████████

89

███
███
███
███

████████████████████████████████

  ███
███
███
███
███
███

  ███
███
██

      ███
      ██
      ██████████████████████████████████

  ███
███
███
███
██

  ███
███
███
█████████████████████████

4-17

███████████████████████████████████████

██

██

██

██

██

██

██

██████

██

██

██

██

█████████████████████████████████

██

██

███
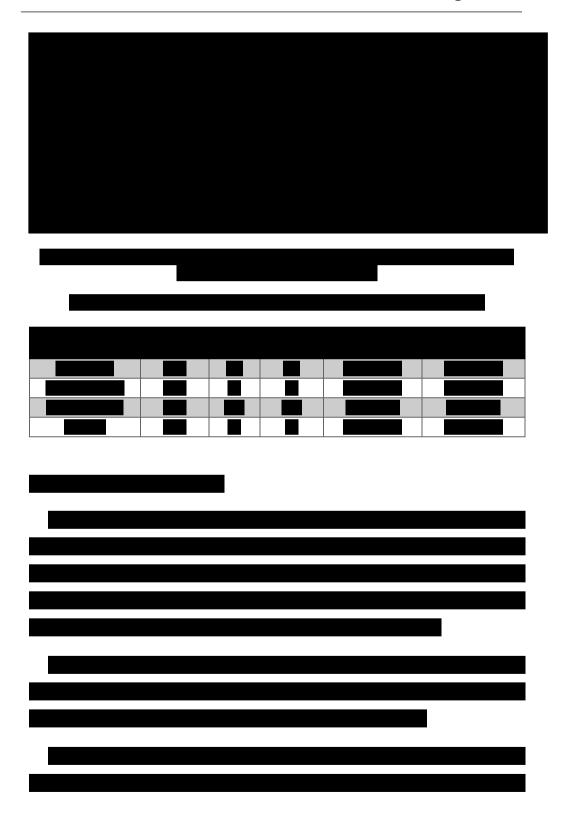
Towards commercial products

██
██
██
██
████████████████

██

██
██
██
██
██
██████████████████████████████████████

███
██████████████

███	███	███	███	███	███	███	███	███
███	███	███	███	███	███	███	███	███
███	███	███	███	███	███	███	███	███
███	███	███	███	███	███	███	███	███
███	███	███	███	███	███	███	███	███
███	███	███	███	███	███	███	███	███
███	███	███	███	███	███	███	███	███
███	███	███	███	███	███	███	███	███

███
██
██
████████████████████████████████████

██

██

██

███████████

███

██

██

██

██████████████████████

███

██

██

██

██

██

██

██

██

██

119

██
███████

██	██	██	██	██	██	██

███

██

██

██

██

██████████

████████████████████████████

███

██

███

███

██

██

██

██

██

████████████████████████

███

██

██

██

121

███████████████████████

██
███
███
██
██
███
██
██████████████████████████████████████

██
██
██
██
██
██
██
████████████████████

████████████████████████████████████

██

██
██

██
██
██
██

Chapter 4

134

██
      ███
      ███

██
      ███
      ███

██
      ███████████████████
      ███
      ██

██
      ███
      ███████████████████████████

██
      █████

██
      ██

██

██

██

██
      ███████████████████████████

███
      ██

██
      ███
      ██

██
      █████

███
      ███████████████████████████

██.

135
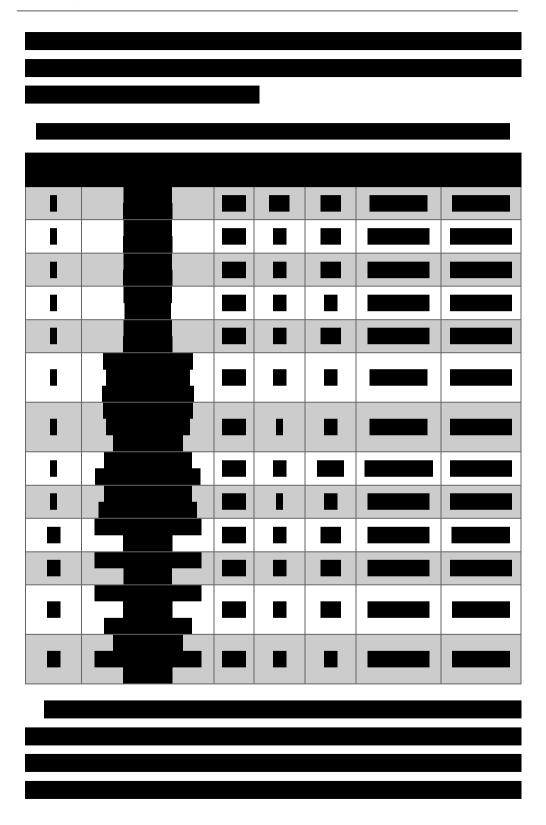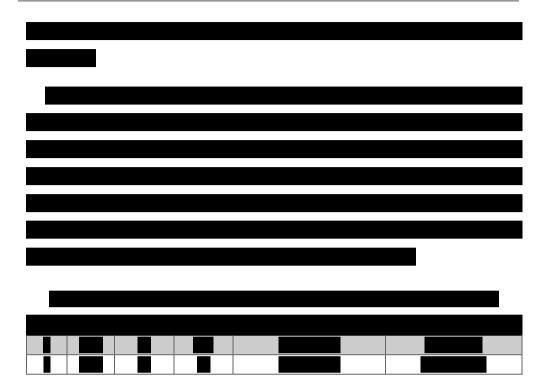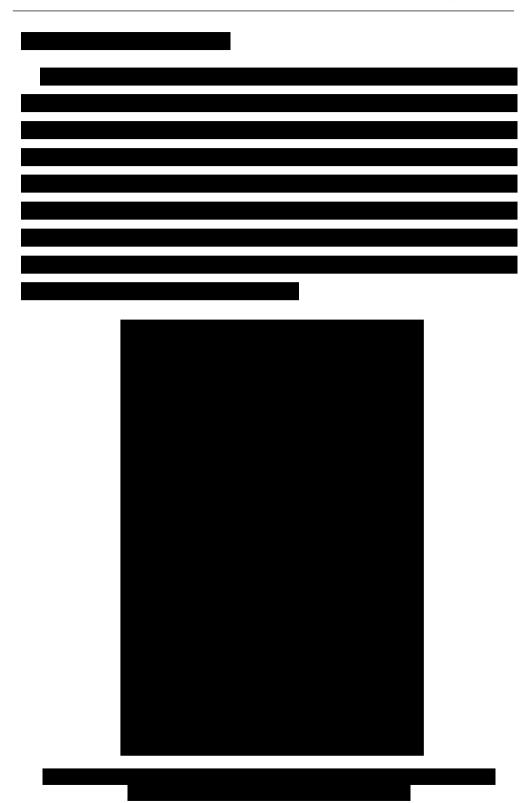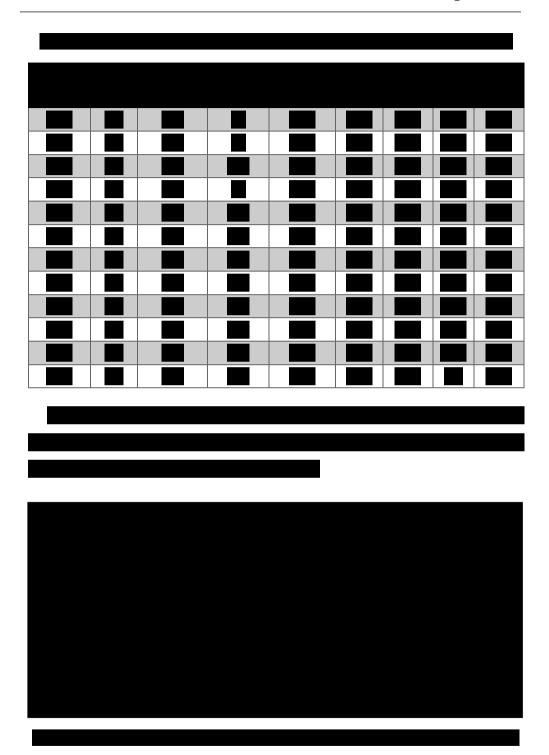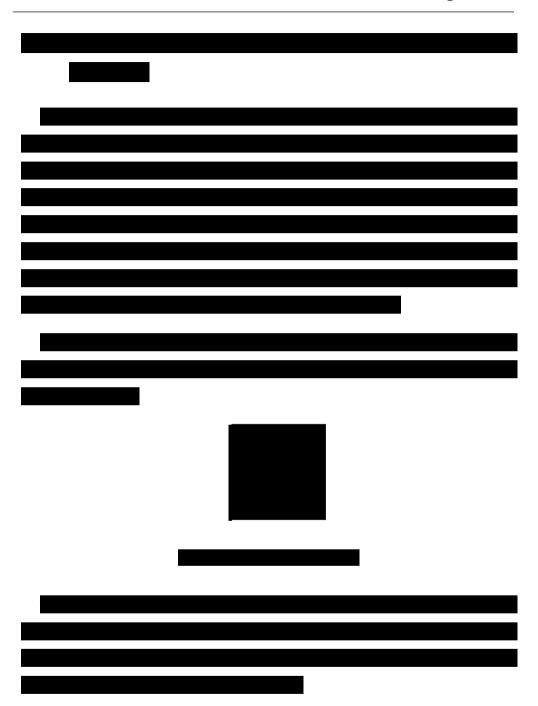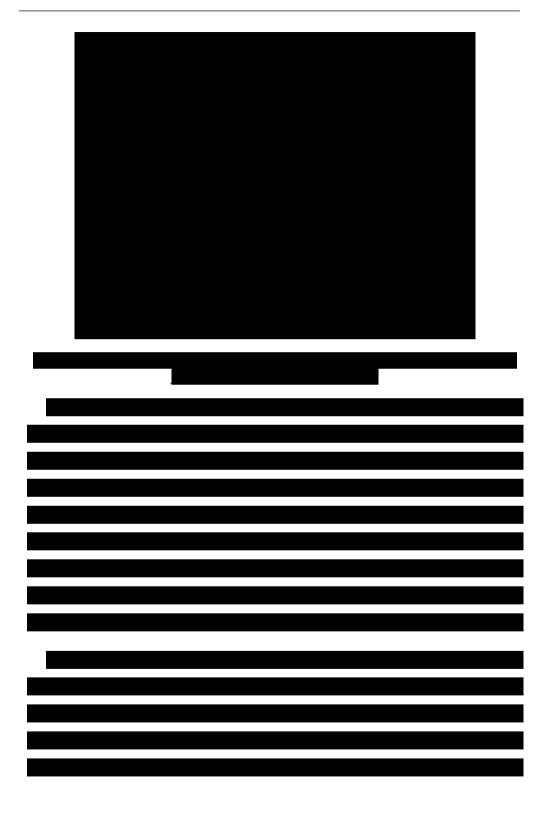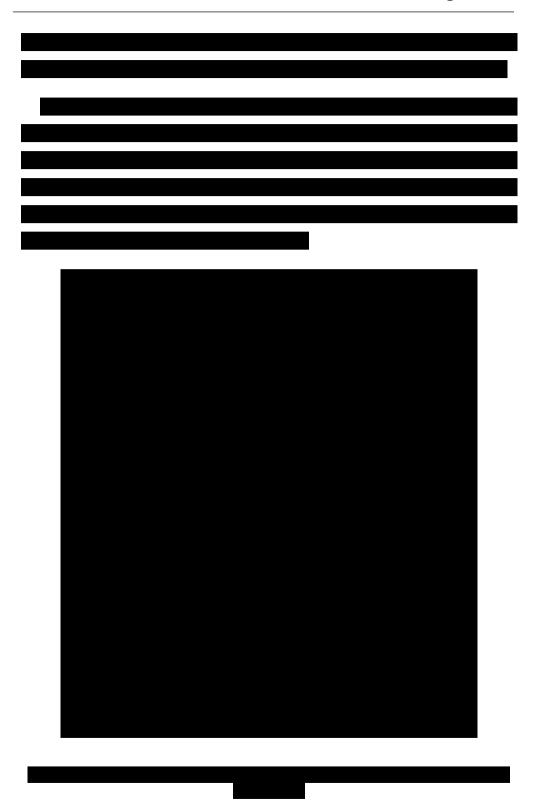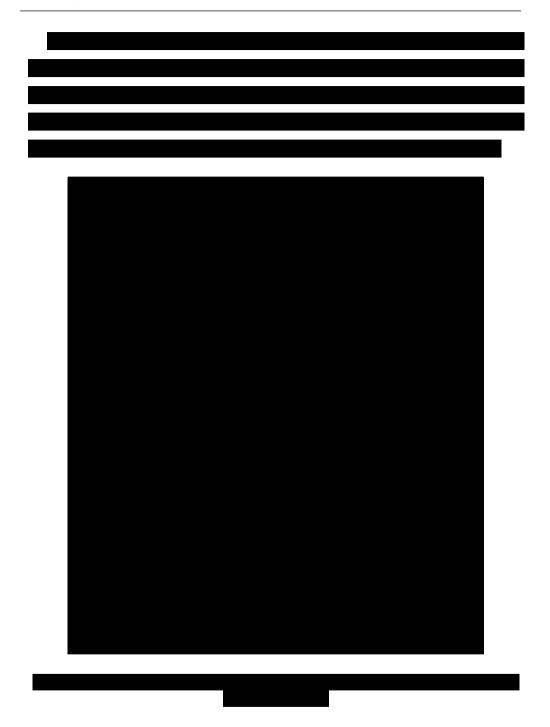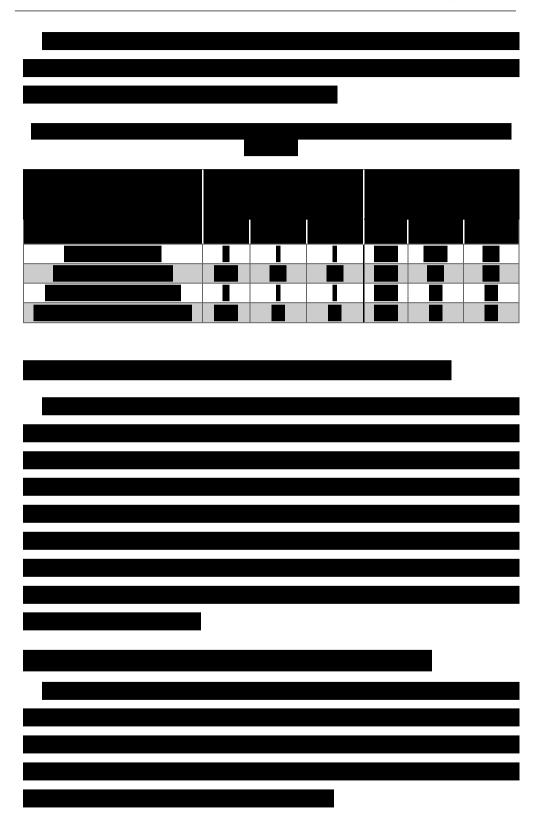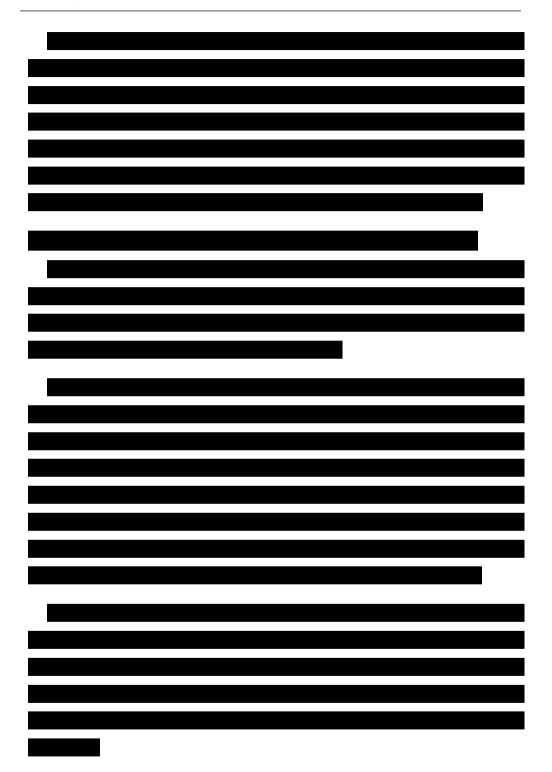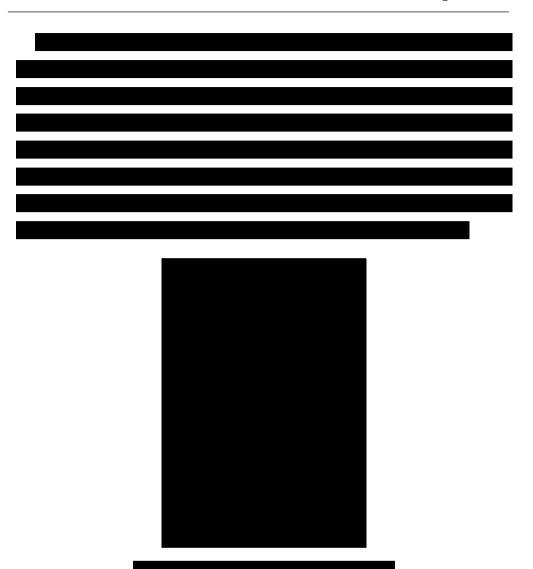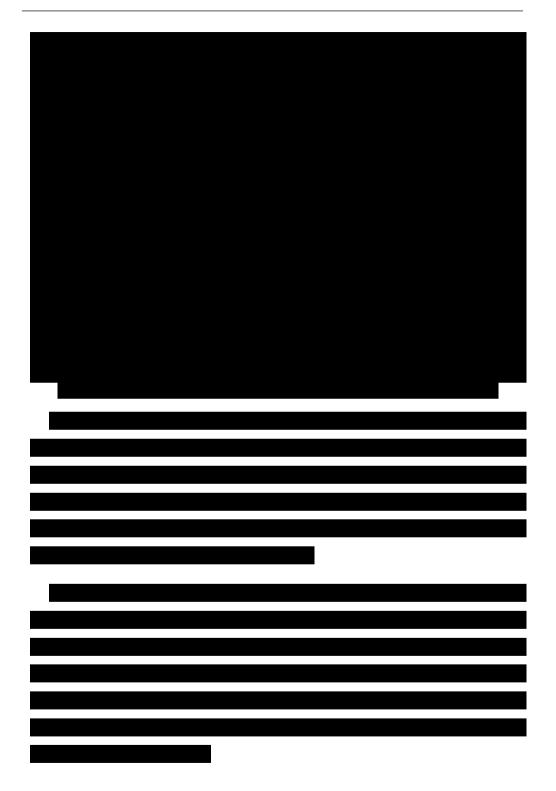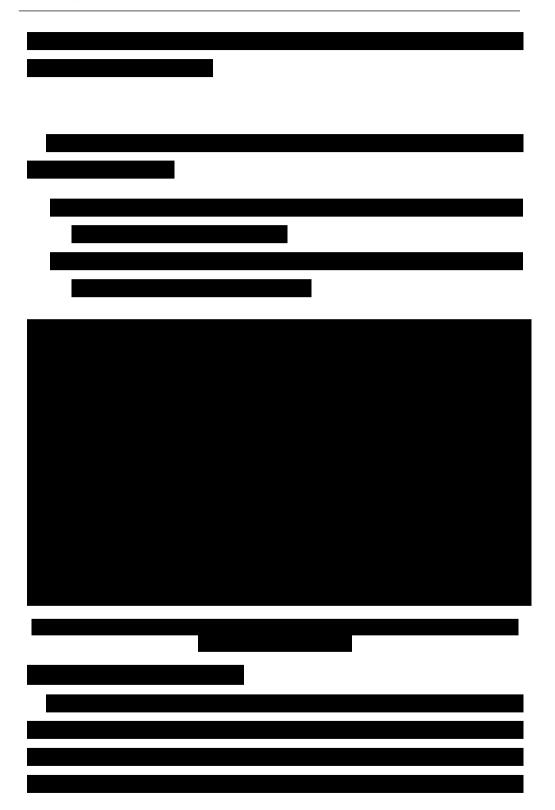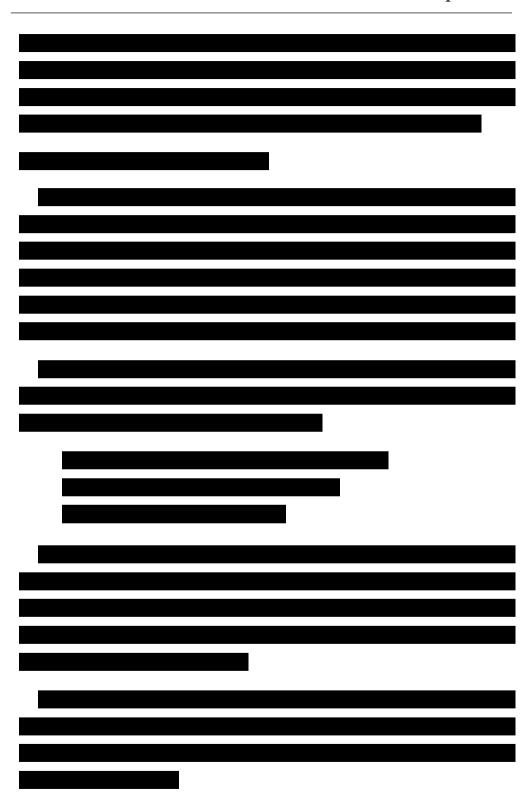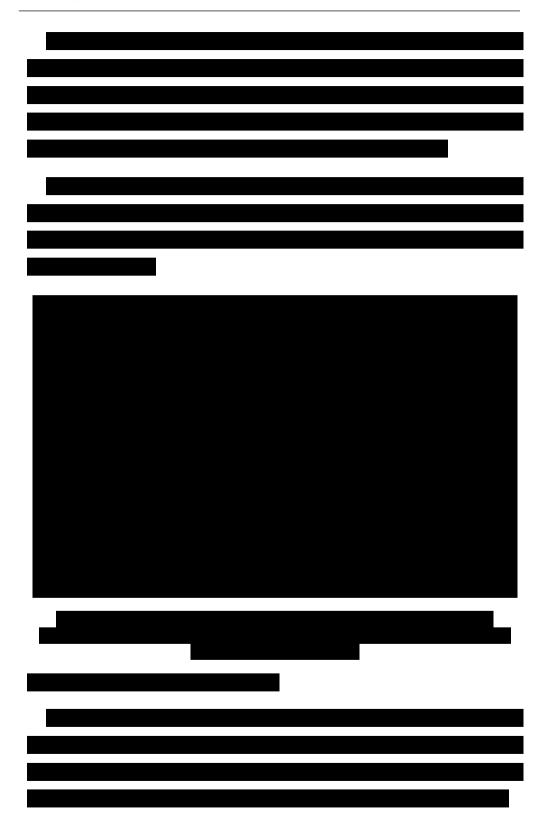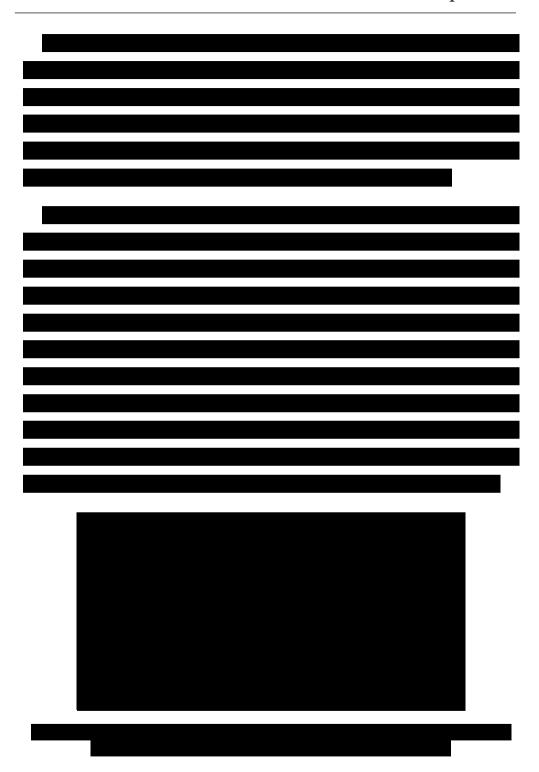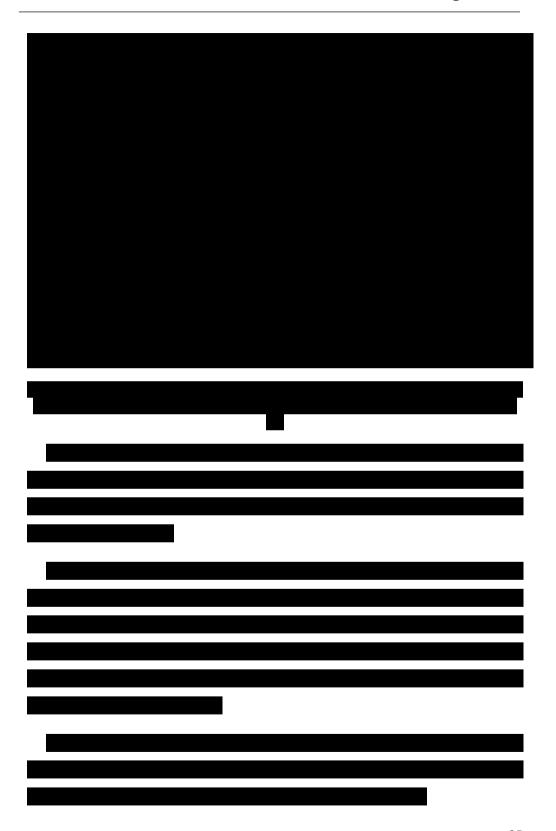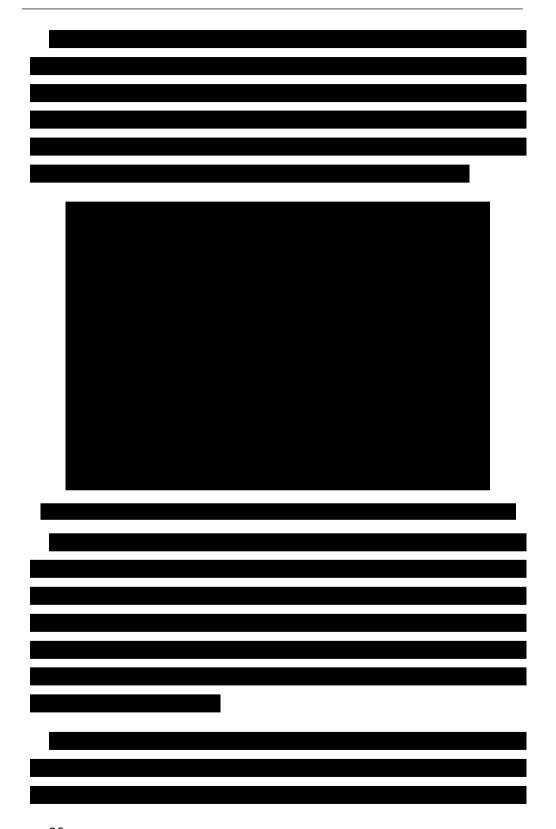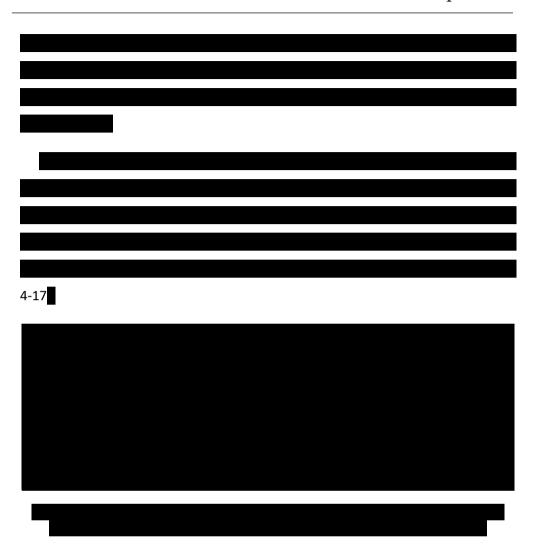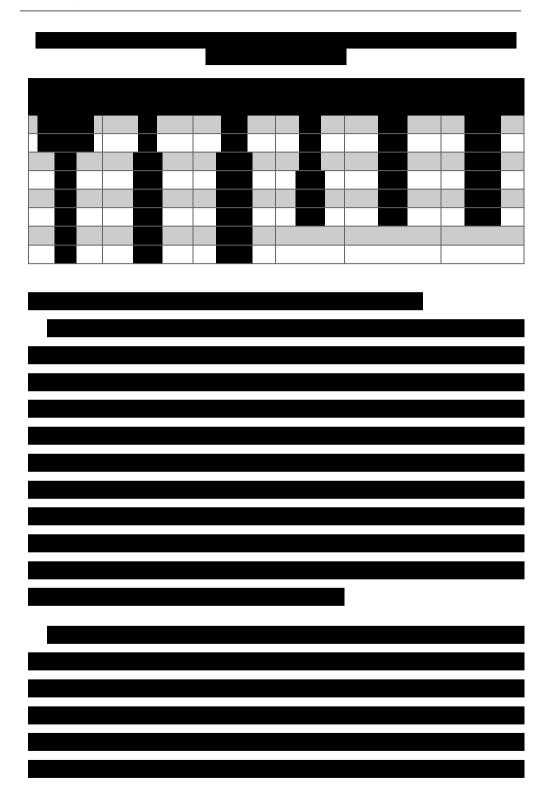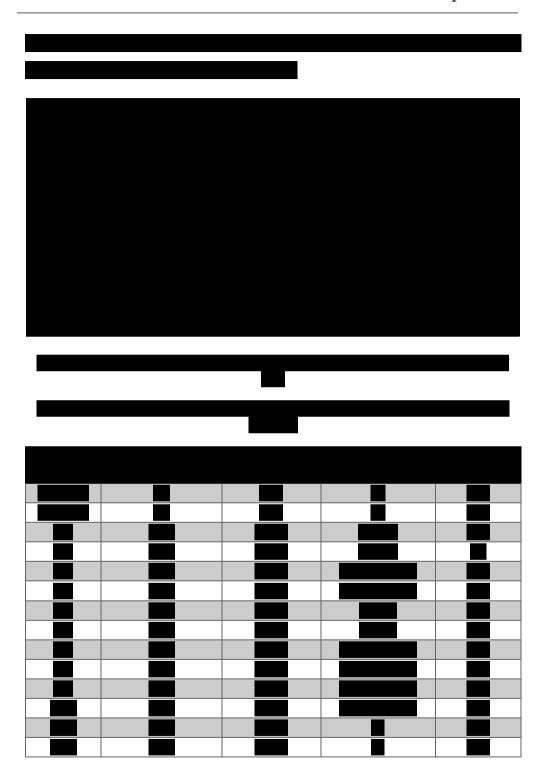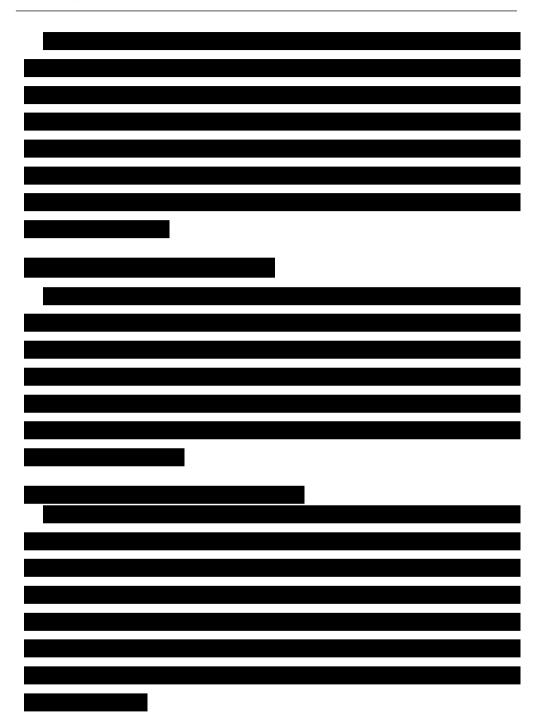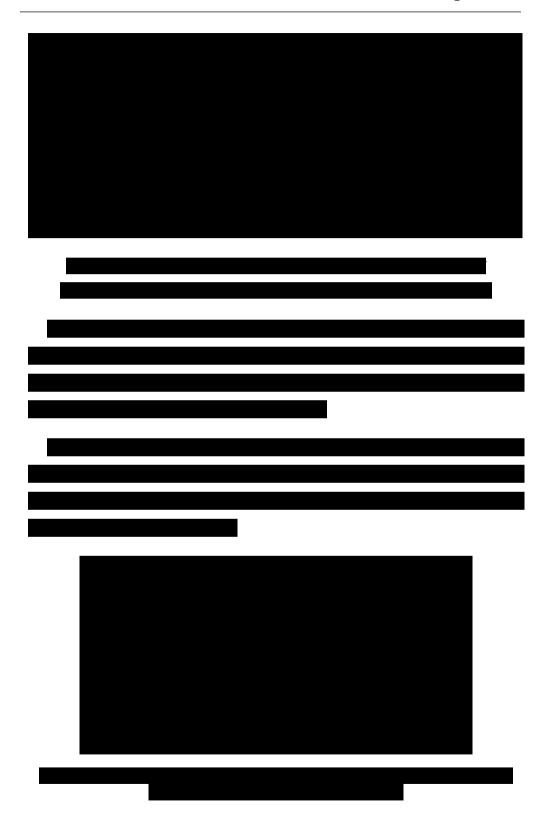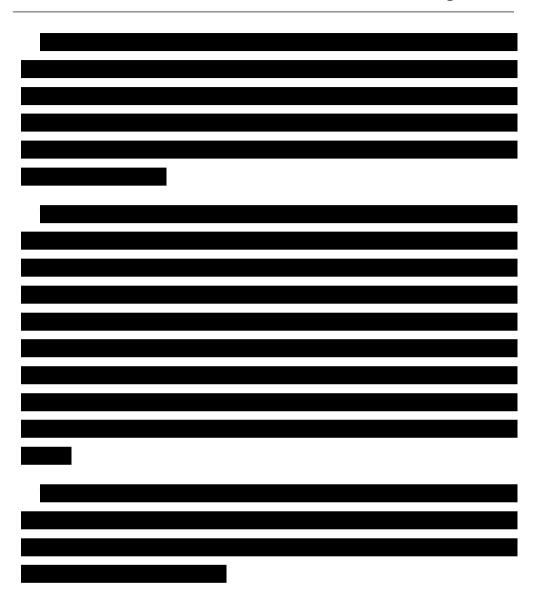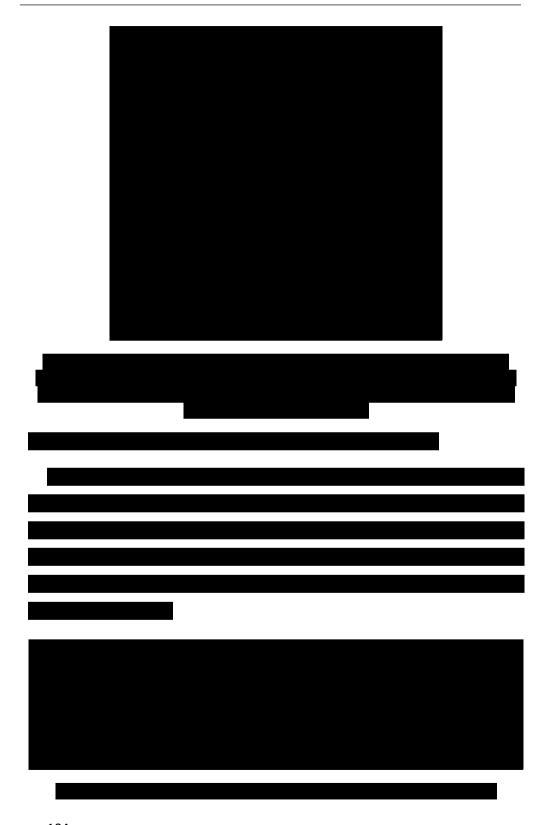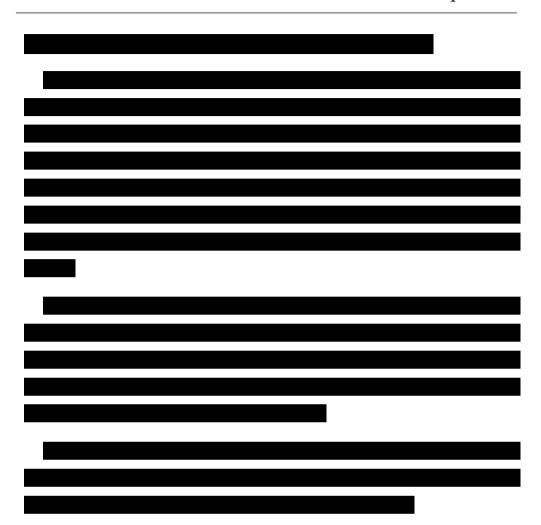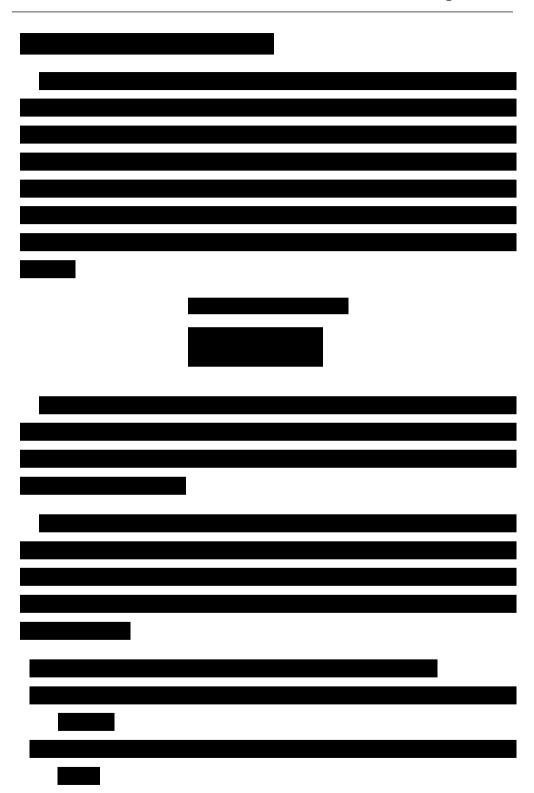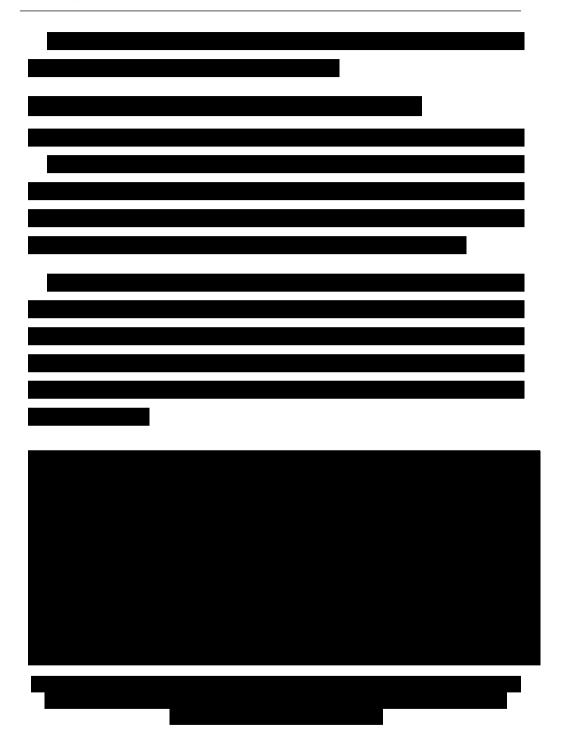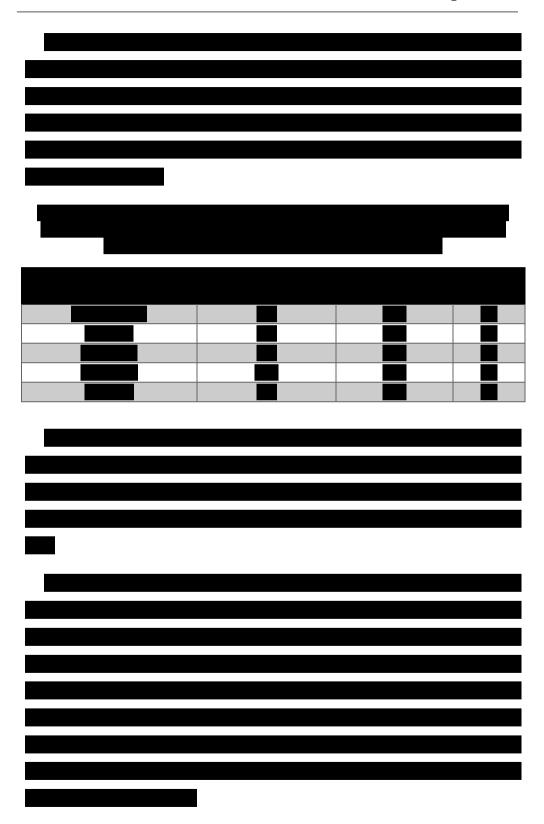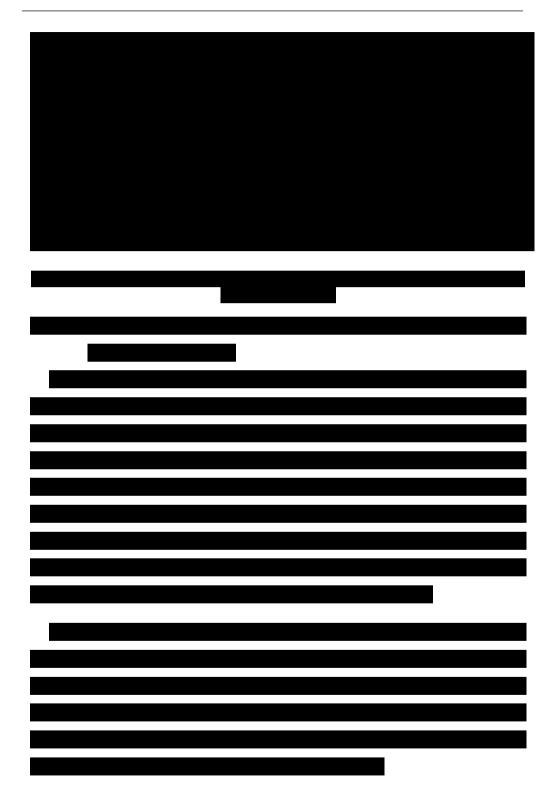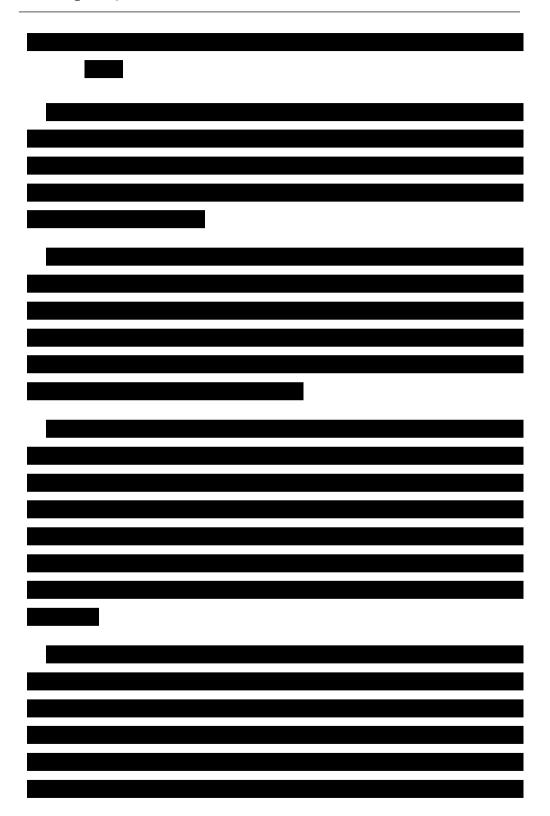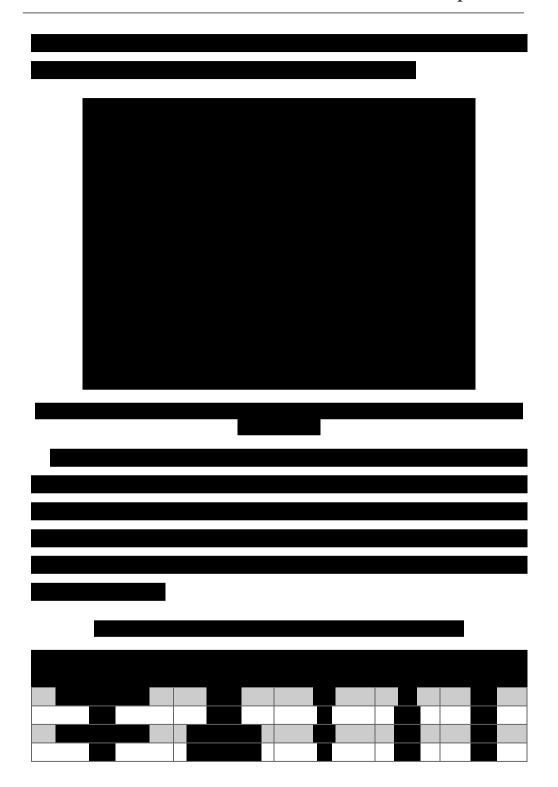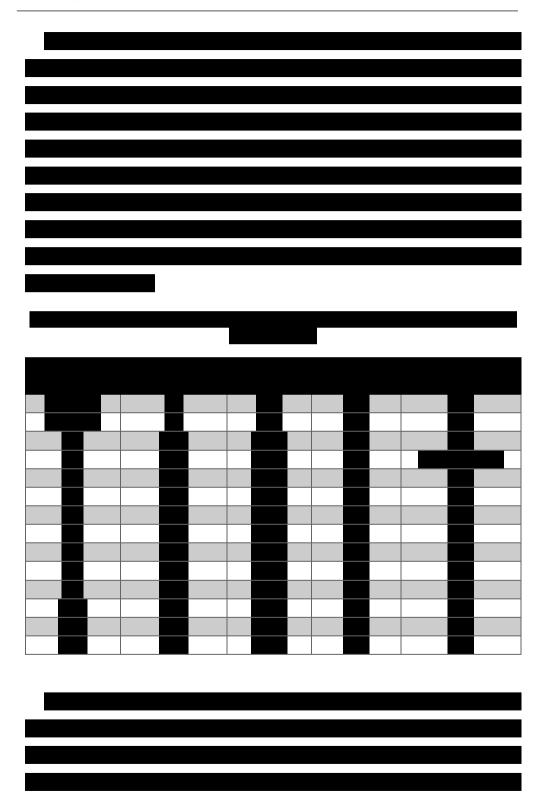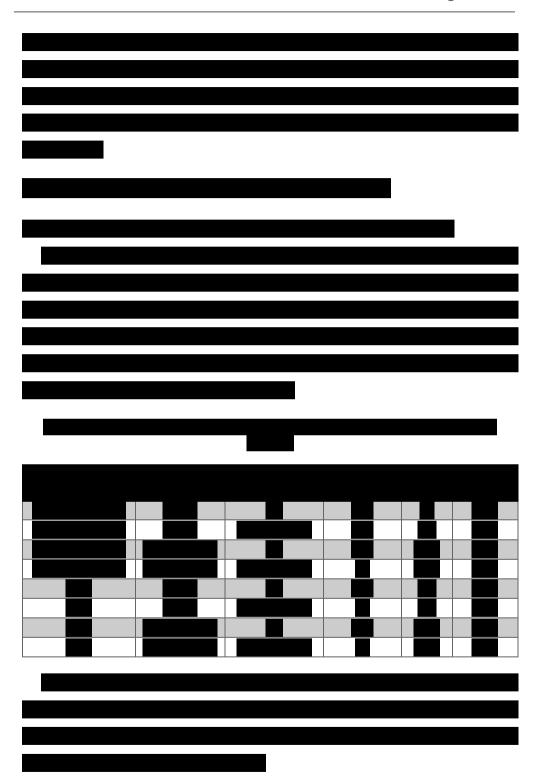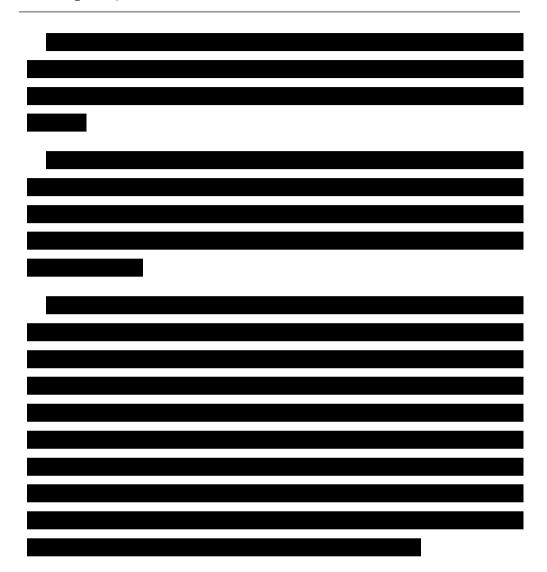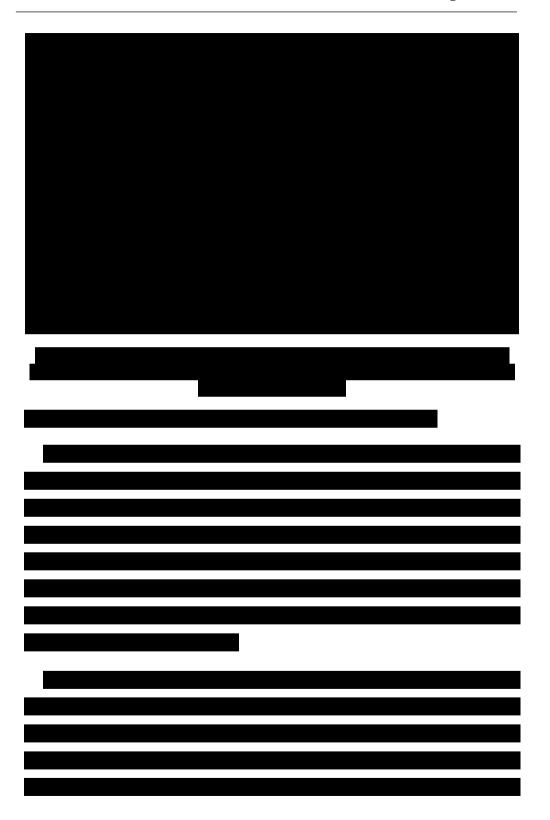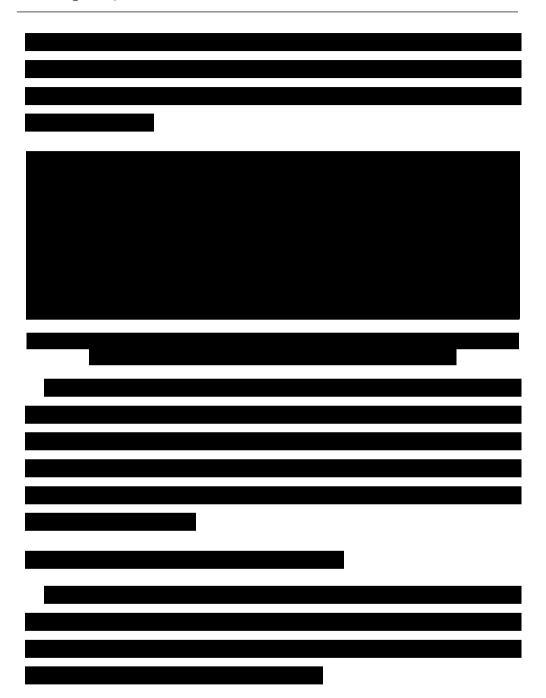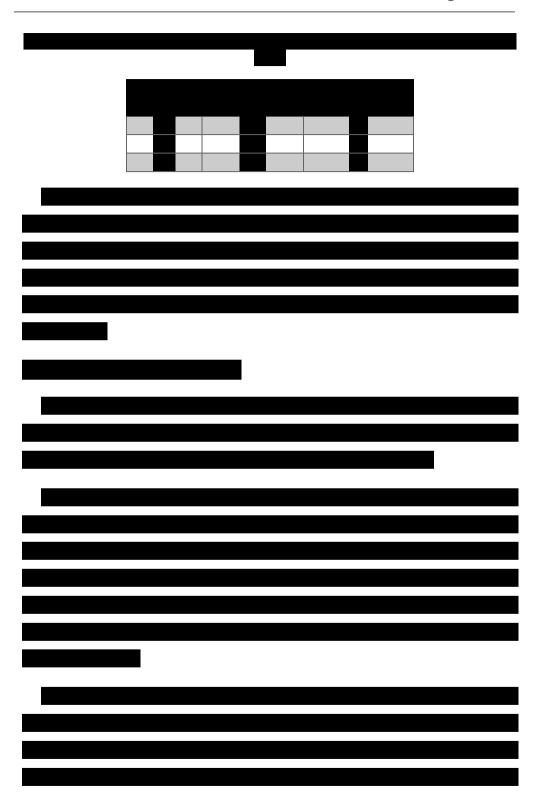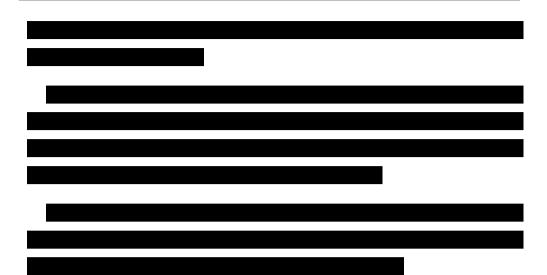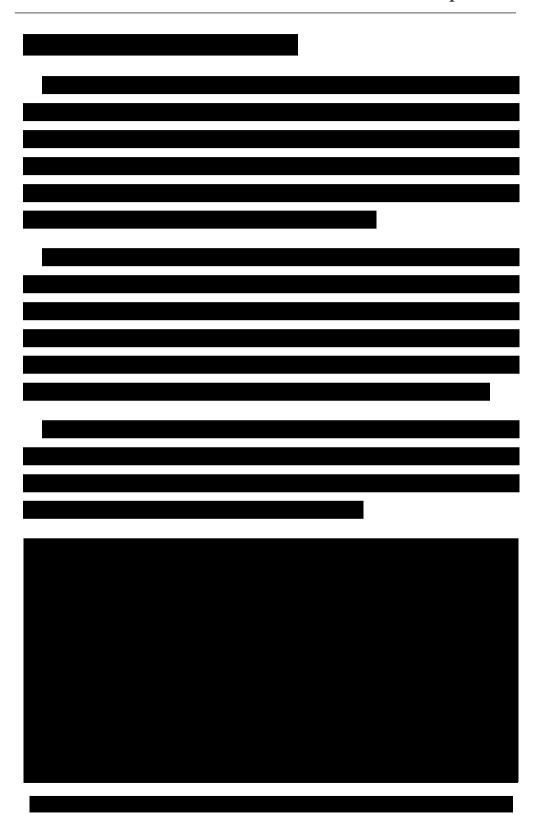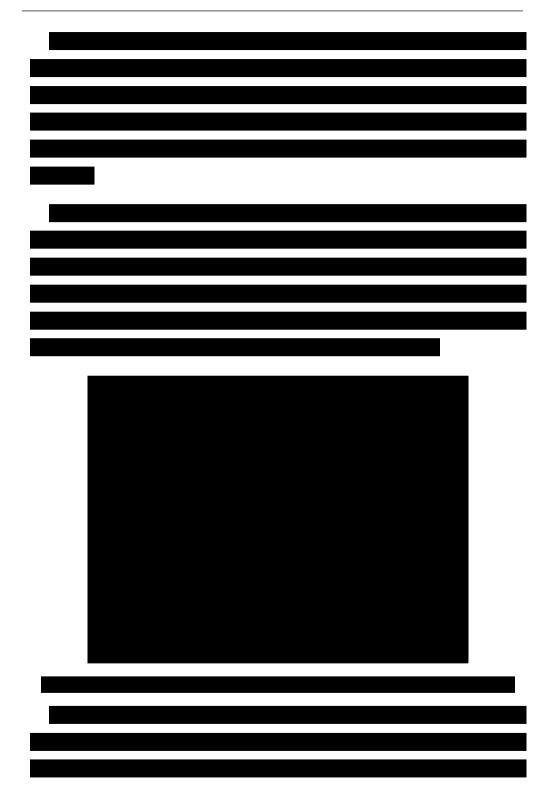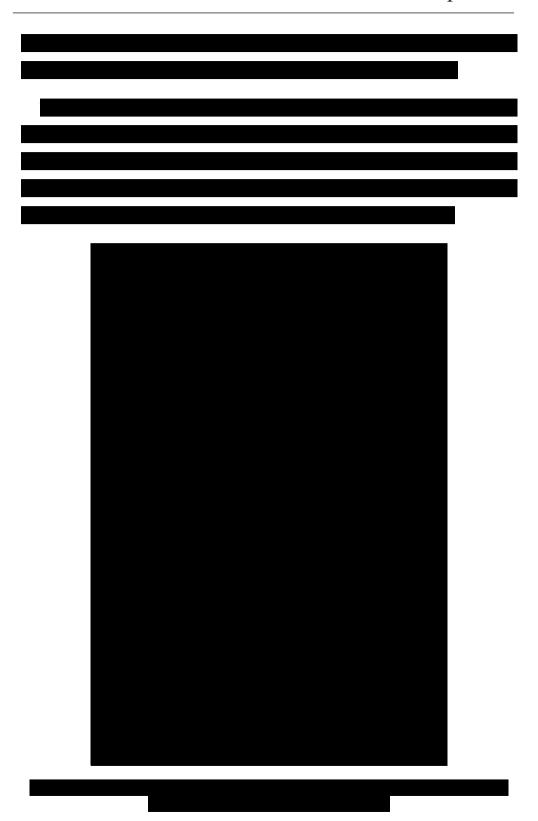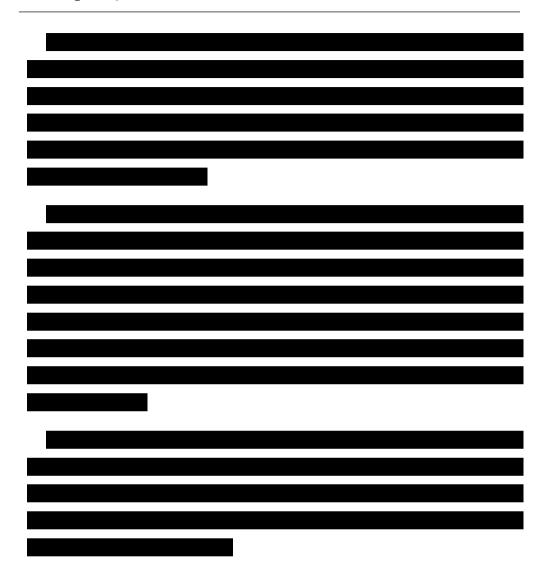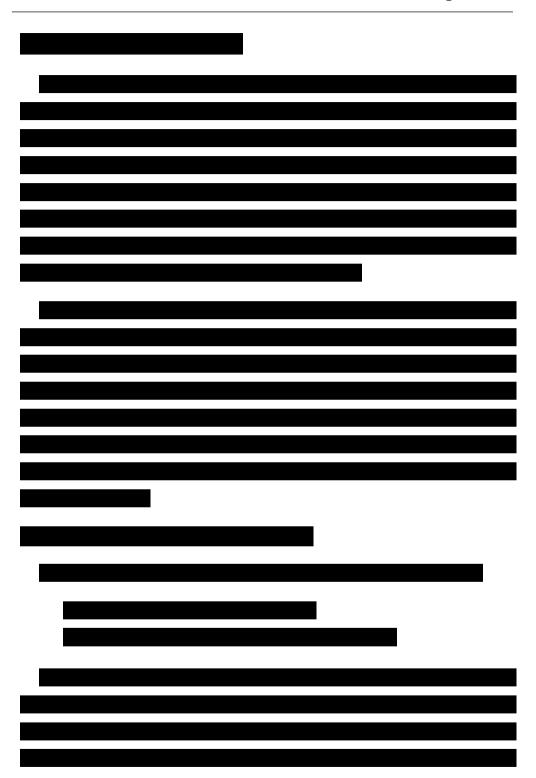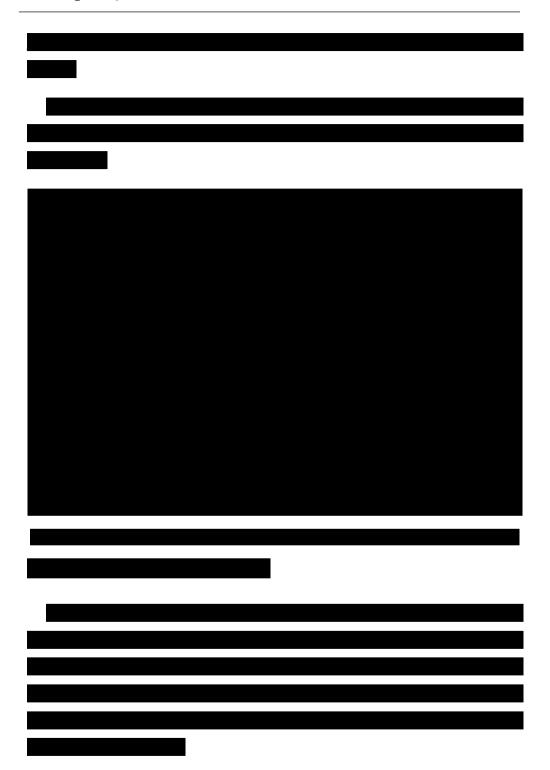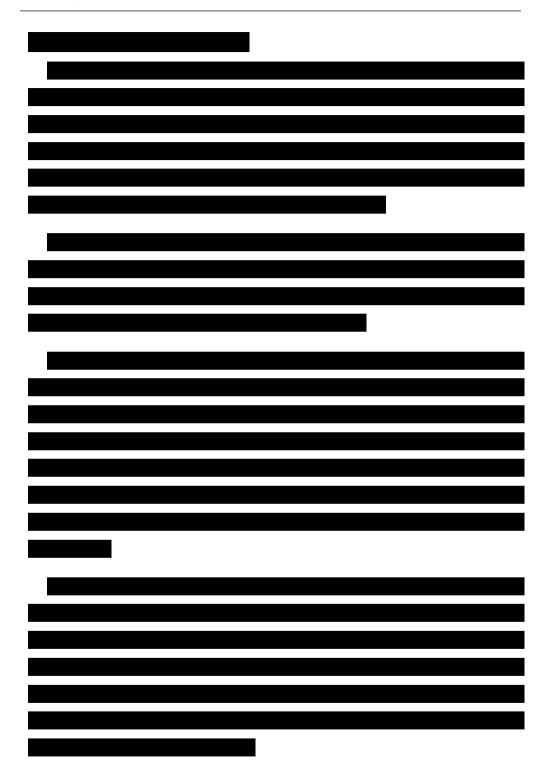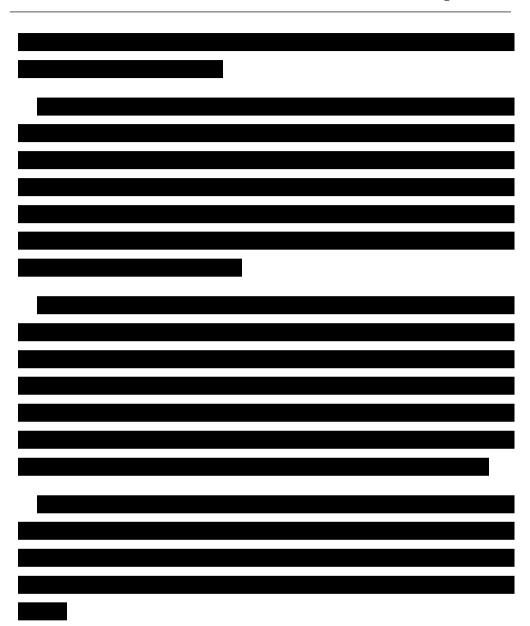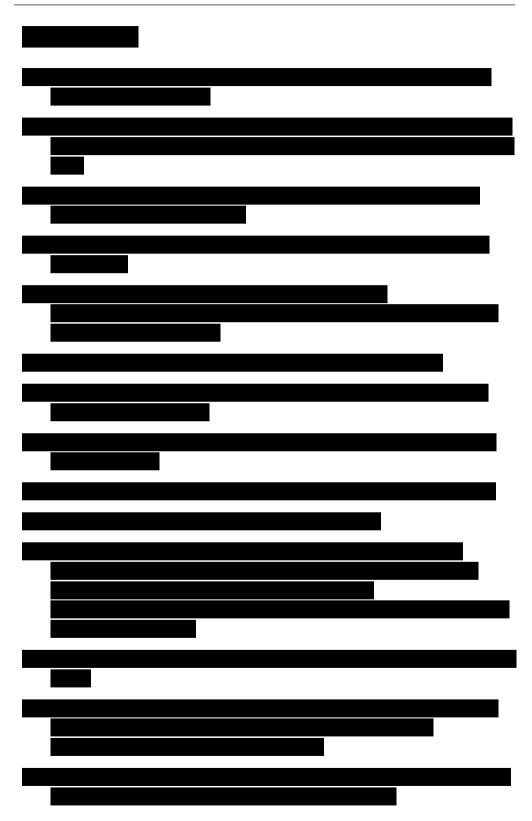
Working prototypes

5   Working prototypes

After developing the NEE photochromic films fulfilling the key properties commonly required for many applications involving transparent photochromic products (e.g. ophthalmic lenses, smart windows, etc.), different prototypes containing NEE photochromic films were prepared.

These prototypes serve as a first proof of concept for the viability of this technology in the different applications and provided to Futurechromes S.L. tangible products that could be exploited to contact possible industrial partners and encourage investments in innovative technologies involving NEE photochromic films.

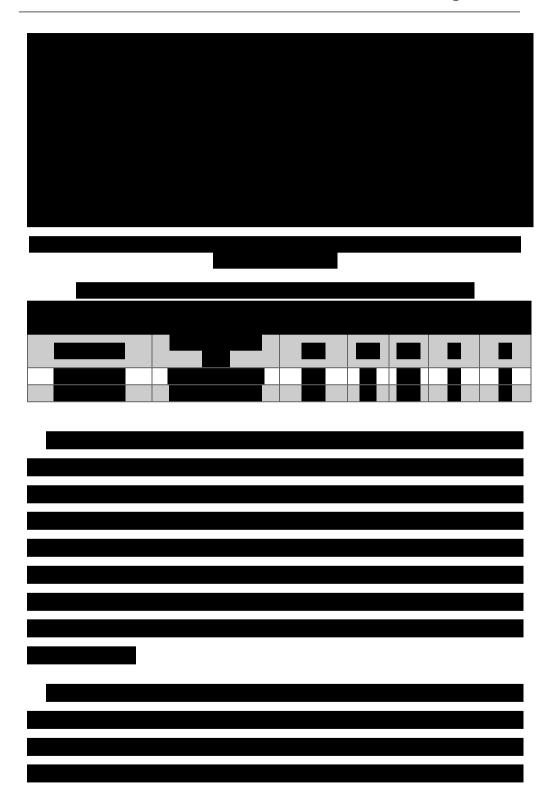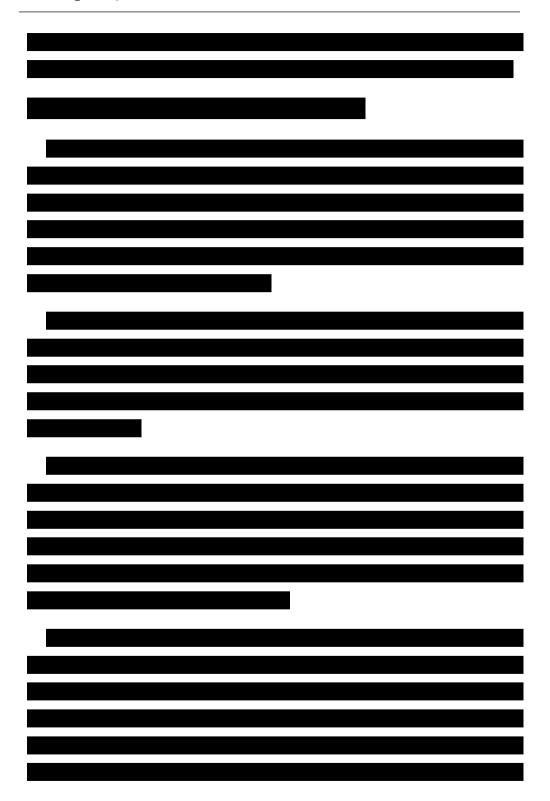The produced prototypes belong to three different industrial categories:

1)   Sports and fashion sun-wear glasses.
2)   Automobile industry.
   a.   A photochromic visor for a motorbike helmet.
   b.   A car model with tinted windshield.
   c.   Antiglare mirror.
3)   Construction glazing.
   a.   A smart window for energy saving.
   b.   A house model, comprising photochromic windows and sky ceiling.

5.1   Photochromic sun-wear glasses

Though the photochromic NEE films technology may still need some improvement for ophthalmic applications, this technology is mature enough for less demanding applications, such as sport and fashion sunglasses, for example. This type of eye-wear has not to be worn constantly since are not prescribed by an ophthalmologist, and therefore users tolerate higher haze values, as it can be extracted by the measurements of commercial glasses (**Table 5-1**).

A prototype of sunglasses was prepared with photochromic NEE films prepared as shown in **section 4.3.2**, and then laminated between two optical lenses using UV-curing resin as glue (see experimental **section 7.4.1** for more details). These lenses were then cut in the appropriate shape and placed into a glasses frame by an ophthalmologist. As a benchmarking, two prescription photochromic lenses and two cycling photochromic glasses were bought and characterized to compare to our prototype.

Images of the Futurechromes S.L. sunglasses prototype in the unactivated and activated form are showed in **Figure 5-1**. The performance comparison respect to commercial photochromic lenses are presented in **Table 5-1**.

Figure 5-1: working prototype of NEE based photochromic sunglasses, indoors and outdoors.

Table 5-1: benchmarking for ophthalmic and sun-wear applications

Brand	Product	Type	Haze (%)	ΔOD	t$_{1/2}$ (s)	t$_{3/4}$(s)
██	██	██	██	██	██	██
██	██	██	██	██	██	██
██	██	██	██	██	██	██
██	██	██	██	██	██	██
██	██	██	██	██	██	██

This small benchmark study showed that prescription glasses had lower haze and higher ΔOD than the sport glasses, but slower fading rates. The NEE film containing prototype had higher haze than sports lenses. However, it must be considered that the glasses lenses were hand made in our laboratory (the initial NEE films had lower haze than the product). Well established industrial techniques would guarantee a decrease of the haze.

On the other hand, the prototype containing the NEE films had a high ΔOD, comparable to the prescription lenses, and fading rates faster than the sports lenses, where this parameter is rather critical. Therefore, this technology is likely to have a competitive advantage respect both prescription and sports glasses, once an industrialized product process is developed.

5.2 Automobile industry prototypes

The use of photochromic materials in automobile applications was theorized for decades. Although plenty of patents applications on photochromic windshields exists,[1–4] this field seems to lack commercial momentum and enrolment of automobile producers, with these preferring technologies such as electrochromic glass,[5,6] possibly due to the slow kinetic response of currently existing photochromic glazing. Only after-market photochromic films that can be installed

on windows or windshields directly by the users seem to have some commercial activity.[7,8]

On the contrary, lighter and simpler devices like motorcycling helmet visors seem to favor photochromic technologies since they do not require wiring nor power supply.[9] Since the kinetic response is (literally) of vital importance for automotive applications, the boost in photochromic kinetics of NEE films could provide an interesting breakthrough in this sector.

As examples for the automotive industry, three prototypes were prepared. A motorcycle helmet visor was covered with a photochromic NEE film made by the doctor blade casting technique (**Chapter 4.5.3**). The windshields of a toy car were coated with photochromic nanoemulsion to generate the NEE films in-situ. An antiglare mirror was prepared also by direct coating of a polished aluminum mirror with photochromic nanoemulsion.

Photographs of these prototypes when placed indoors and outdoors are shown in **Figure 5-2**. The photochromic performances of the helmet visor and antiglare mirror is presented at **Table 5-2**. In the case of the mirror the reflectance (R%) variation is determined rather than the typical transmittance.

Table 5-2: Summary of the photochromic performances of helmet visor and antiglare mirror prototypes: average transmittance and reflectance in the visible range (700-400 nm), and fading kinetics.

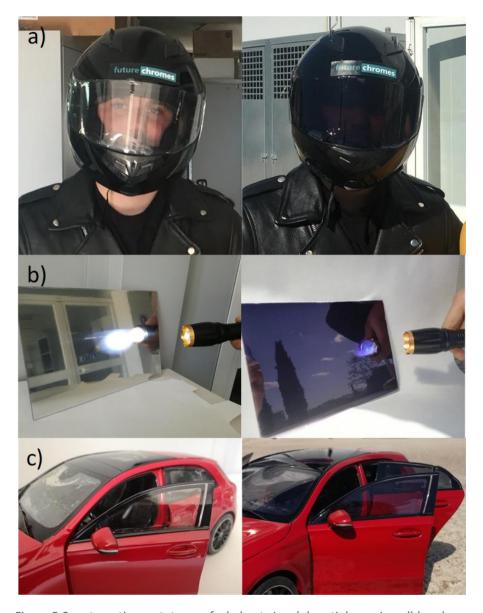| Sample	Aver. unactivated visible T% / R%	Aver. activated visible T% / R%	$t_{1/2}$ (s)	$t_{3/4}$ (s)

Figure 5-2: automotive prototypes of a helmet visor (a), antiglare mirror (b) and car windshields (c), indoors and outdoors.

5.3   Construction glazing

Glass is a key component of modern buildings. Generally found in windows and sky-ceilings, it allows to separate spaces, regulate air flow and gather sun light and warmth, all while providing sight through it. However, traditional glazing presents clear limitations, like its poor insulating properties and tendency to break. Plenty of innovative technologies exist to improve its strength,[10,11] and insulating glass units (IGU) can be generated, with multiple glass layers separated by an inert gas or vacuum, to increase the thermal isolation.[12,13] It is also possible to introduce new properties to the glass, like anti-glare and hydrophobic coatings, or lowering the infrared emissivity (Low-E) for further improved thermic isolation.[13–15]

A particular class of innovative glazing called Smart Windows (**SW**) are characterized by being able to adapt their transmittance to the weather conditions.[14,15] These SW are usually designed as an IGU that provide thermal isolation, and a chromogenic material that can change its visible light transmittance in response to external stimuli (e.g. temperature, light, voltage…), granting comfort to the inhabitants of the buildings.[16] This chromogenic material could be passive (photochromic and thermochromic) or active (electrochromic). Since energy irradiated from the sun reaches earth as visible light (44.7%) and heat-generating near-infrared radiation (48.7%),[17,18] SW can potentially save energy consumption by reducing cooling and lighting expenses if designed efficiently.[19,20]

As a first step into this application, a photochromic SW prototype was made to test the feasibility of photochromic NEE films as chromogenic materials for passive SW. This prototype was prepared by casting the nanoemulsion on an IGU made from Low-E glass (**Figure 5-3**).
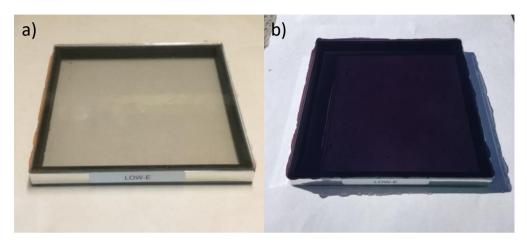

Figure 5-3: photographs of Low-E IGU coated with NEE photochromic film, in the unactivated stated (a) and activated under sunlight (b).

5.3.1   Spectroscopic characterization of photochromic SW prototype

The transmittance spectra of this prototype were measured in the spectral range of solar irradiance, i.e. UV-vis range (300 - 800 nm) and in the NIR (800 - 5000 nm) (**Figure 5-4, magenta**). The range between 1100 and 1500 nm, however, could not be measured with our current NIR detectors. The transmittance of this prototype was compared to the uncoated IGU (**Figure 5-4, blue**), to a clear glass (**Figure 5-4, black**), a NEE coated clear glass (**Figure 5-4, red**), and to a commercial thermochromic SW (**Figure 5-4, green**) provided by InnoGlass Technology Co.[21]

The major difference between the clear glass and the Low-E IGU was found at the NIR spectrum, with the latter transmitting approximately 90 % of light between 800 and 2800 nm, and the former showing a gradual drop in transmittance from 1500 to 2800 nm. The visible transmittance of the Low-E IGU was approximately 15% lower than the clear glass, likely due to the higher reflection caused by the presence of two glass slabs instead of just one. The lower transmittance in the NIR

and the fact that IGU had lower thermal conductivity is what reduces energy consumption.[13]
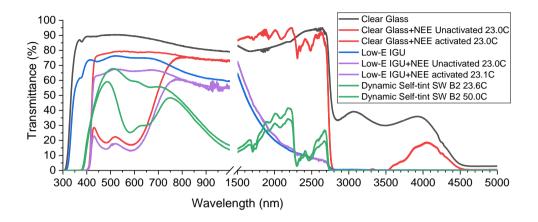

Figure 5-4: UV-vis and Near-IR spectra of clear glass (black), Low-E IGU (blue), a thermochromic SW (magenta) and SW prototypes with NEE films coated on clear glass (red) and on Low-E IGU (green).

When coated with a NEE photochromic film, the NIR transmittance of the clear glass from 2800 nm to 4000 nm decreased significantly, though no noticeable change was observed for the Low-E IGU. The change, however, was more noticeable in the UV and visible ranges. The transmittance decreased about 10 % respect to the respective uncoated glasses when the NEE film was not photoactivated. When irradiated with a solar simulator, the NEE film activated and the transmittance plummeted to 20% for the clear glass and 15% for the Low-E IGU. In the UV range, the photochromic dyes of the NEE films absorbed virtually all light between 200 nm and 400 nm in both the unactivated and the activated states.

When compared to the thermochromic SW, the photochromic SW prototype had similar UV and visible transmittance, being the transmittance of the clear state of our prototype between 10 % and 20 % higher, depending on the specific wavelength (60-70 %). The activated state of the photochromic SW prototype had significantly lower transmittance in the visible range than the thermochromic SW at 50 °C, and had a more neutral coloration. In the Near-IR however, the thermochromic SW had

146

an intense and broad band from 750 nm to 2200 nm, which is not present in our prototype, possibly derived by the characteristics of the thermochromic dye. Above 2200 nm, both the thermochromic SW and the photochromic SW prototype had low (< 20%) or no measurable transmittance.

5.3.2   Thermal isolation experiment

As a proof of concept, a preliminary experiment was performed to evaluate the thermal isolating properties and potential energy savings derived from using photochromic SW integrating NEE films.

A portion of 8 cm per 8 cm on the top face a cardboard box was cut, and covered with the glass samples described above (**Section 5.3.1**) to emulate a window on a building façade. The interior of the box was irradiated through this window with a solar simulator, the power of which at the window surface was 1 sun (1 Kw/m^2). The temperature variation between the interior and the exterior of the box was monitored with probe thermometers **(Figure 5-5, a)**.

The box interior was irradiated for 30 min, after which the solar simulator was turned off and the interior of the box allowed to equilibrate for 30 minutes. The temperature increase inside the box respect to the measured room temperature was calculated and is presented at **Figure 5-5, a**.
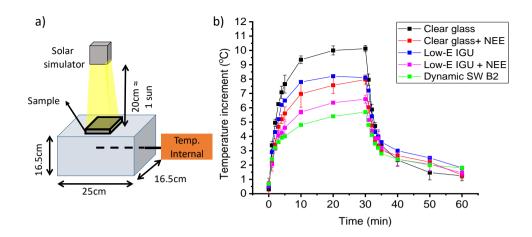
Figure 5-5: scheme of the cardboard box experiment (a) and variation of the temperature inside the box during and after irradiation (b).

As it was expected, the temperature increment observed when using the uncoated clear glass slide as window was the highest (approximately 10 $^{\circ}$C), due to its poor insulating properties. Also expected, the Low-E IGU had a smaller temperature increment (approximately 8 $^{\circ}$C), as this glass reflects a significant portion of the NIR irradiation and the double glass layer of the IGU hinders thermal convection.

The NEE coated clear glass presented a lower increase of temperature respect to the uncoated glass (approximately 8 $^{\circ}$C), as it reduced the heat gained from the visible range of the solar spectrum (filtered by the photoactivated film). Even further insulation was achieved when combining the NEE film with the Low-E IGU, achieving an increment of only 6.5 $^{\circ}$C. This temperature increase was the closest to the observed for the thermochromic SW, which had the smallest increment (approximately 5.5 $^{\circ}$C).

Though this preliminary experiment could hardly correlate to potential energy savings, the reduced temperature increase suggests a smaller usage of cooling and air conditioning devices in hot/warm weather conditions. Moreover, it provided an interesting comparison of the NEE coated samples with commercial glazing

technologies, pointing out the photochromic NEE films as a promising alternative for passive SW and innovative glazing, to achieve both comfort improvement and energy savings.

5.3.3   Building model for aesthetic display

A house model was prepared as a *functional* prototype. The model was made from wood and removable glass slides coated with photochromic films that resemble windows and sky ceiling. This films were made though the NEE technology or the standard procedure to embed photochromic dyes directly in polymeric matrices. The photochromic films onto the glass slides contain the most promising photochromic dyes packages in terms of color neutrality, colorability and/or kinetic response. If better dyes will be available in the future, the glass slides could be easily substituted with the new ones (**Figure 5-6**).

Figure 5-6: photograph of the photochromic glass-containing building model.

This model will serve to show to possible partners the tunability of the NEE technology and the improved photochromic performances compared to existing technologies.

5.4   References

[1]   A. A. Yavuz, B. Glas, M. Ihle, H. Hacioglu, K. Wehefritz, *Adjustable Tint*, **2014**, US20150253594A1.

[2]   L. Olenick, *Photochromic Automobile Windows*, **2014**, US2014011812A1.

[3]   E. R. Love, B. J. Love, *Solar Windshield System*, **2003**, US6536828B2.

[4]   D. L. Casey, *Photochromic Windshield*, **2017**, US2017/0100993A1.

[5]   Gentex, "Aircraft Windows, Gentex," can be found under https://www.gentex.com/aerospace/aircraft-windows, last access: November **2019**.

[6]   Continental Automotive, "Continental Automotive - Intelligent Glass Control," can be found under https://www.continental-automotive.com/en-gl/Passenger-Cars/Interior/Comfort-Security/Intelligent-Glass-Control, last access: November **2019**.

[7]   Tintdepot, "Photochromic Window Film (Transitional)," can be found under https://tintdepot.com/product/photochromic-window-film-2/, last access: November **2019**.

[8]   Coolvu, "Transitional Window Film – CoolVu," can be found under https://www.coolvuwindowfilm.com/photochromic-transitional-window-film/, last access: November **2019**..

[9]   "SHOEI® Transitions® Shields," can be found under https://www.transitions.com/en-ca/products/transitions-adaptive-shields/shoeisupsup-transitionssupsup-shields/, last access: November **2019**.

[10] K. L. Barefoor, J. J. Price, J. M. Quintal, R. L. Stewart, *Strengthened Glass Articles and Methods of Making*, **2009**, WO2010/016928A2.

[11] C. M. Fernández-Posada, A. R. Barron, *J. Non. Cryst. Solids* **2019**, *518*, 1.

[12] B. P. Jelle, A. Hynd, A. Gustavsen, D. Arasteh, H. Goudey, R. Hart, *Sol. Energy Mater. Sol. Cells* **2012**, *96*, 1.

[13] W. J. Hee, M. A. Alghoul, B. Bakhtyar, O. Elayeb, M. A. Shameri, M. S. Alrubaih, K. Sopian, *Renew. Sustain. Energy Rev.* **2015**, *42*, 323.

[14] S. D. Rezaei, S. Shannigrahi, S. Ramakrishna, *Sol. Energy Mater. Sol. Cells* **2017**, *159*, 26.

[15] E. Cuce, S. B. Riffat, *Renew. Sustain. Energy Rev.* **2015**, *41*, 695.

[16] Y. Wang, E. L. Runnerstrom, D. J. Milliron, *Annu. Rev. Chem. Biomol. Eng.* **2016**, *7*, 283.

[17] B. P. Jelle, S. E. Kalnæs, T. Gao, *Energy Build.* **2015**, *96*, 329.

[18] H. Khandelwal, A. P. H. J. Schenning, M. G. Debije, *Adv. Energy Mater*. **2017**, *7*, 1602209.

[19] M. Mahdavinejad, M. Bemanian, N. Khaksar, *Int. Conf. Comput. Commun. Manag.* **2011**, *5*, 335.

[20] A. Piccolo, F. Simone, *J. Build. Eng.* **2015**, *3*, 94.

[21] InnoGlass, "Película intercalar Autointetizado dinámico y Smart Glass – InnoGlass: película inteligente, vidrio inteligente, vidrio intercambiable, vidrio de privacidad, película PDLC, LCD transparente ¡Especialista!," can be found under https://www.innoglass.es/vidrio-inteligente-auto-tinte/, last access: November **2019**.
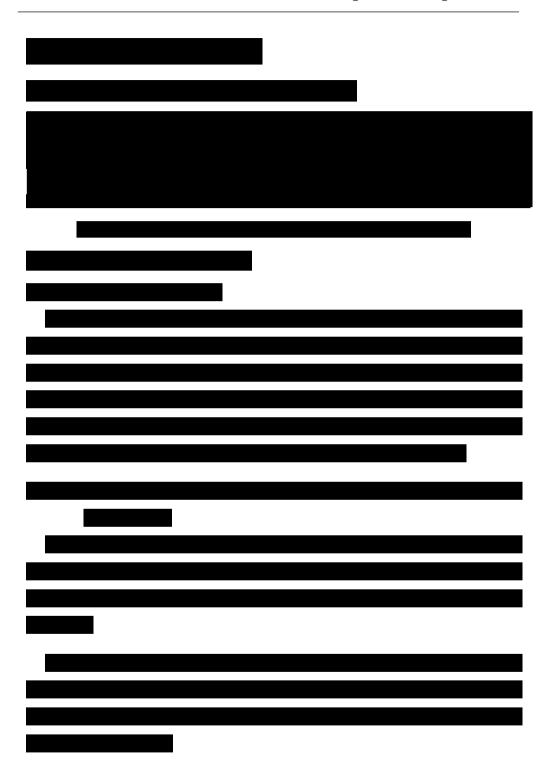
Chapter 6

Conclusions

6   Conclusions

In this doctoral research, a solid photochromic material with fast photochromic response and high visible transparency is presented, based on the nanoemulsion entrapment technology. The developed material is now suitable for optically clear industrial applications such as smart windows and eyewear. The universality of this platform has been proven for a variety of commercially available T-type photochromic dyes, oils and polymeric matrices, which allowed the tuning of its photochromic and mechanical properties to meet industrial specific requirements.
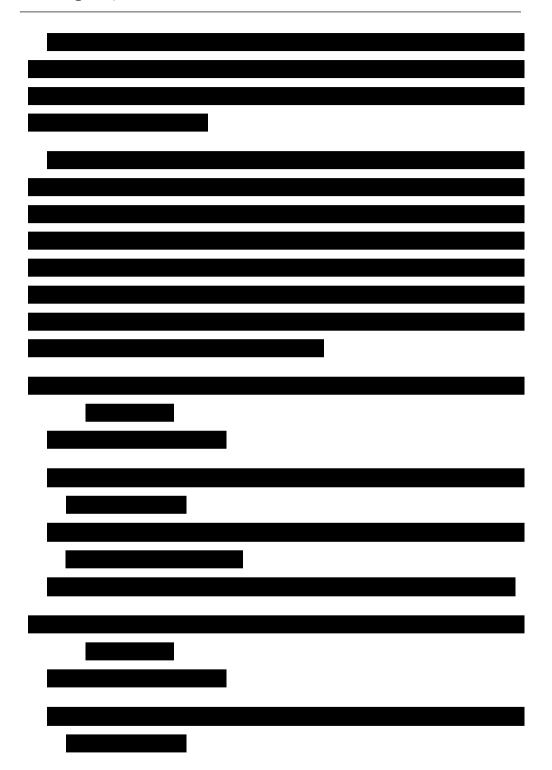
The photochromic films were successfully produced to match the specific requirements of the glass and ophthalmic industry ███████████████████ ██ ██ ██ ██ ██ ██ ███
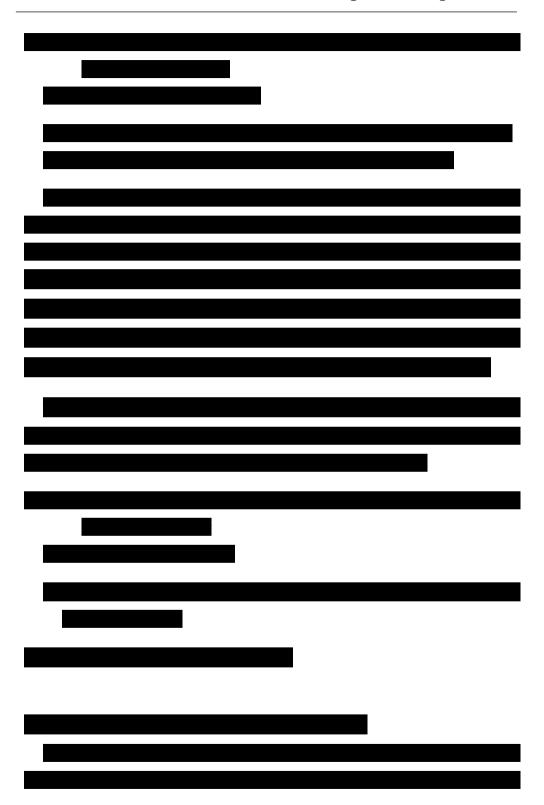
Meanwhile, photochromic films based on the nanoemulsion entrapment technique were introduced into working prototypes of sunglasses, smart windows and a motorcycling helmet visor. Functional prototypes of construction glass and windshields were also prepared using building and car models. These prototypes were used for benchmarking, comparing them to some photochromic products currently available in the market, showing promising results and competitive advantages for the nanoemulsion entrapment based products. These prototypes are currently used as demonstrators by Futurechromes S.L. to contact industrial manufacturers and partners to promote the commercialization of innovative products based on the nanoemulsion entrapment technology.

Chapter 7

Experimental procedure

███████████████████████████████████

███

███
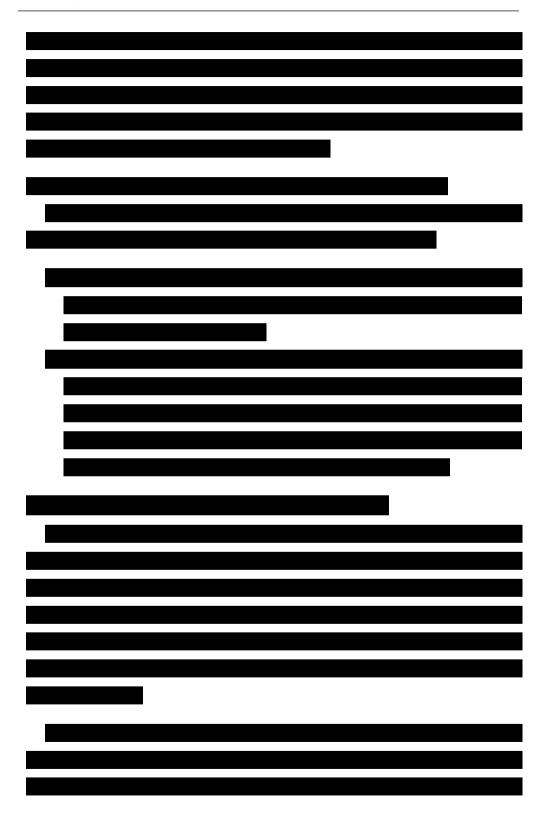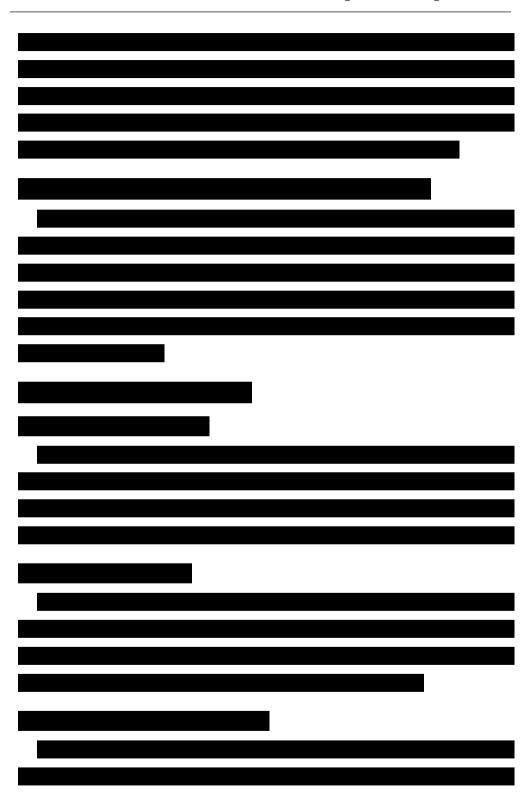
████████████████

███

██

██

██

████████

███

██

██

██

██

██████████████████████████████████

██

███

██

█████████████████████████████████

██████████████████████████

███████████████████████

██

███

██

██

████

███████████████████████

███

██

██

██

██

███

██████████████████

███

██

██

██

██████████████████████████

██████████████████████████

███

██

██████████████

███████████████

███

██

██

██

███████████████████████████████

███

██

██
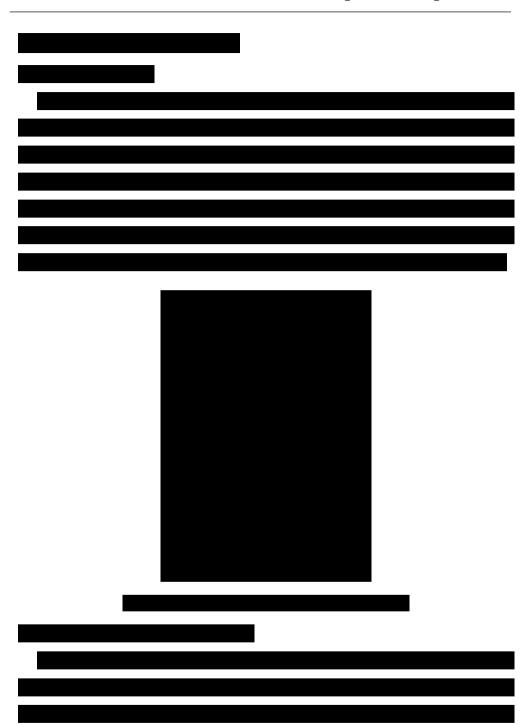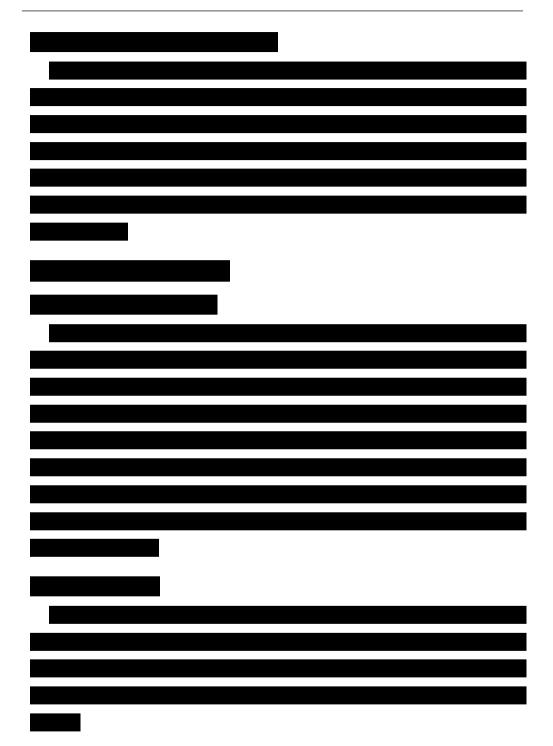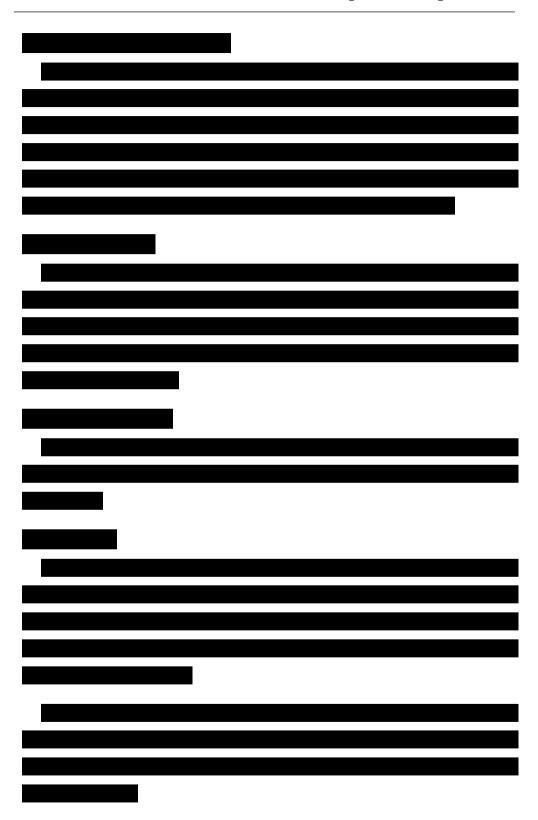
███████████████████████
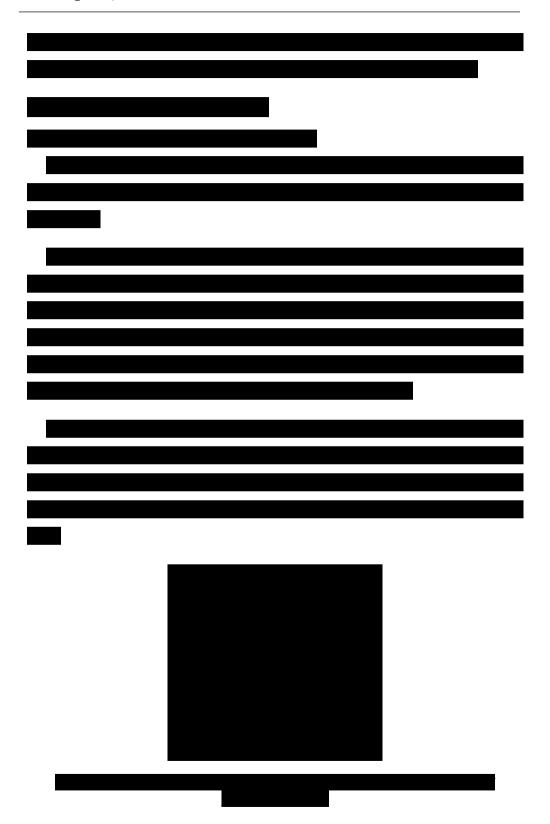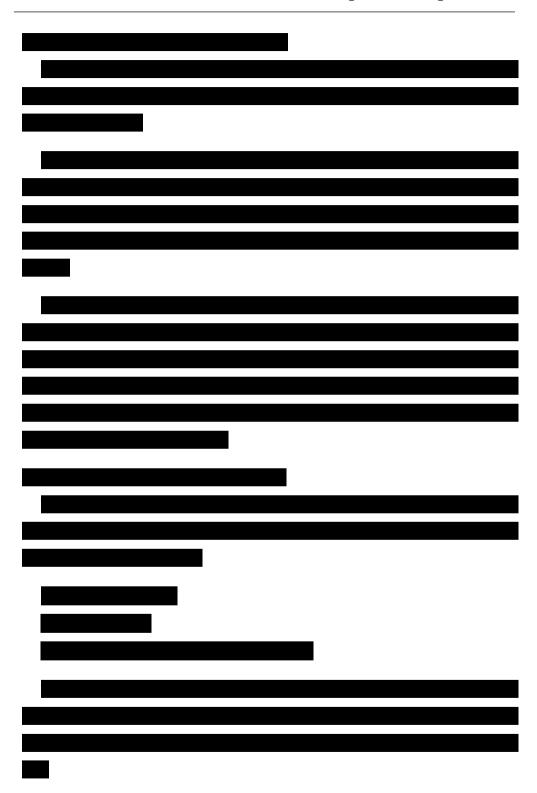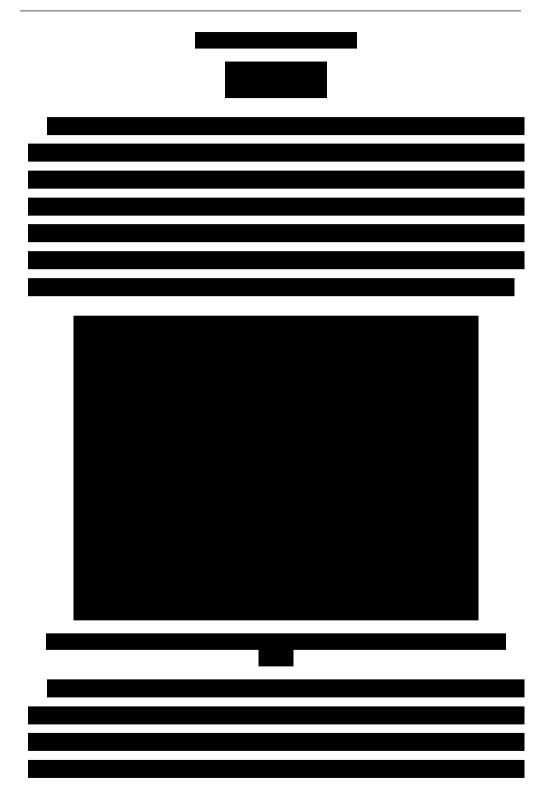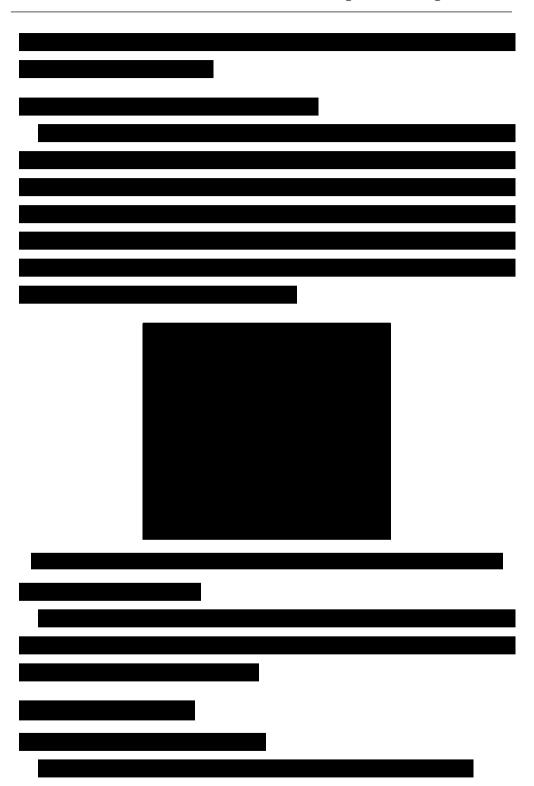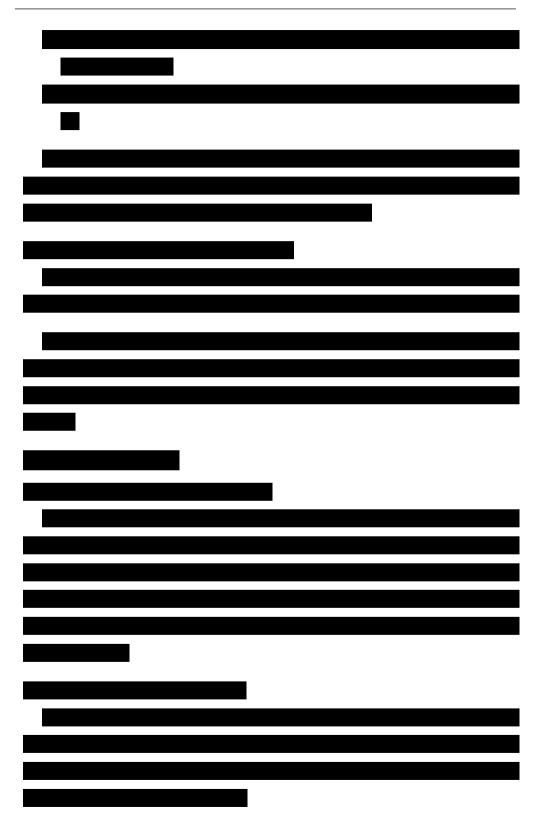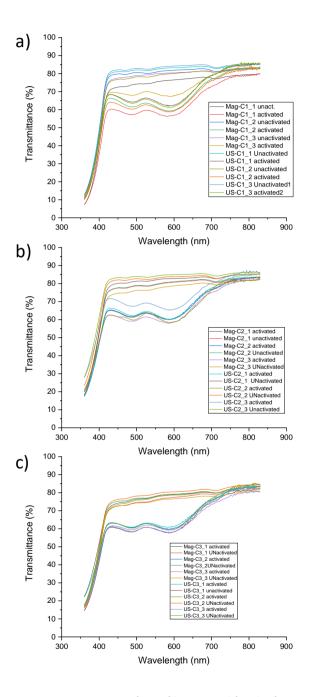
8   Annexes

Figure 8-1: Transmittance spectra of NEE films casted for the first time (a), after one recycling step (b), and after one recycling step (c).